EARTH SURFACE PROCESSES AND LANDFORMS
Earth Surf. Process. Landforms (2014)

Published online in Wiley Online Library
(wileyonlinelibrary.com) DOI: 10.1002/esp.3657

Alternate bars in a sandy gravel bed river: generation, migration and interactions with superimposed dunes

Stephane Rodrigues,[1]* Erik Mosselman,[2] Nicolas Claude,[3] Coraline L. Wintenberger[1] and Philippe Juge[4]
[1] E.A. 6293 GéHCO, GéoHydrosystèmes Continentaux, Faculté des Sciences et Techniques, Université François Rabelais de Tours, Tours, France
[2] Deltares and Delft University of Technology, Delft, The Netherlands
[3] Laboratoire d'hydraulique Saint Venant, ENPC, EDF R&D, CETMEF, Université Paris-Est, Chatou, France
[4] CETU ELMIS, Centre Universitaire de Chinon, Chinon, France

Received 9 June 2013; Revised 15 September 2014; Accepted 22 September 2014

*Correspondence to: Stephane Rodrigues, E.A. 6293 GéHCO, GéoHydrosystèmes Continentaux, Faculté des Sciences et Techniques, Université François Rabelais de Tours, Parc de Grandmont, 37200 Tours, France. E-mail: srodrigues@univ-tours.fr

ESPL
Earth Surface Processes and Landforms

ABSTRACT: A field study was carried out to investigate the development of alternate bars in a secondary channel of the Loire River (France) as a function of discharge variations. We combined frequent bathymetric surveys, scour chains and stratigraphical analysis of deposits with measurements and modelling of flow dynamics. The channel exhibited migrating bars, non-migrating bars and superimposed dunes. Possible mechanisms of bar initiation were found to be chutes associated with changes of bank direction and instability resulting from interactions between existing bars during the fall in water level after floods. We propose that the reworking of bar sediments during low flows (high width-to-depth ratio β), reinforced by high values of the Shields mobility parameter, can explain the formation or re-generation of new alternate migrating bars during a subsequent flood. The migration pattern of the bars was found to be cyclic and to depend mainly on (i) channel layout and (ii) the dynamics of superimposed dunes with heights and lengths depending on location and discharge value. For instance, the hysteresis affecting the steepness of dunes influences the flow resistance of the dunes as well as the celerity of migrating bars during flood events. We compare the findings from the field with results from theoretical studies on alternate bars. This gives insight in the phenomena occurring in the complex setting of real rivers, but it also sheds light on the extent to which bar theories based on idealized cases can predict those phenomena.

KEYWORDS: sandy-gravelly rivers; alternate bars; field study; geometrical discontinuities; width-to-depth ratio; bar theory; dune roughness; Loire River; discharge variations; fluvial morphology

Introduction

The formation of alternate bars is a striking phenomenon in fluvial morphology. Alternate bars consist of consecutive diagonal fronts with low-slope riffles located upstream. They are characterized by a bar mode equal to one, in contrast to the higher bar modes of multiple bars (Ikeda, 1984; Jaeggi, 1984). Alternate bars have been studied extensively in laboratory experiments (Fujita and Muramoto, 1985; Struiksma and Crosato, 1989; Tubino, 1991; Lisle *et al.*, 1993; Lanzoni and Tubino, 1999; Lanzoni, 2000; Knaapen *et al.*, 2001; Crosato *et al.*, 2011) and theoretical analyses (reviewed later), but studies of their formation and further development in real rivers have remained limited (Welford, 1994; Eekhout *et al.*, 2013). Theoretical analyses of the mathematical equations for flow, sediment transport and morphological bed evolution show that alternate bars occur only within a specific range of the width-to-depth ratio of an alluvial channel. Multiple bars occur in wider and shallower channels, whereas no bars at all occur in narrower and deeper channels. A linear stability analysis provides values of temporal growth rate, migration speed, wavelength and spatial damping factor (Hansen, 1967; Callander, 1969; Blondeaux and Seminara, 1985; Struiksma *et al.*, 1985). It also provides information on relative amplitude changes in time and space, but no absolute quantitative information on amplitudes. The latter is obtained from weakly non-linear stability analysis (Colombini *et al.*, 1987; Schielen *et al.*, 1993). Formally, both linear and weakly non-linear stability analysis hold for infinitesimally small amplitudes and hence apply, strictly speaking, to the initial stage of bar formation only.

Two special cases arise from two different simplifications of the general linear stability analysis. Hansen (1967), Callander (1969) and Blondeaux and Seminara (1985) assume the spatial damping factor to be equal to zero, so that all bars have the same height. This implies they assume an infinitely long channel without any influence from upstream or downstream boundaries. The alternate bars start growing spontaneously at the same time everywhere, without gradients in bar amplitude. The resulting migration speed and wavelength correspond to the bars with the largest temporal growth rate. The alternate bars of this first special case are called 'migrating bars', 'migrating free bars' or, less precisely, 'free bars' (Tubino *et al.*, 1999). Struiksma *et al.* (1985), however, assume that the temporal growth rate and the migration rate are equal to zero, which means that the bars neither migrate nor grow or decay in time. This is assumed to represent bars that are induced by some local non-migrating geometrical forcing, such as a transverse dam in part of the cross-section or an abrupt change in channel curvature. The alternate bars of this second special case are called 'steady bars', 'non-migrating bars', 'spatial bars' or, less precisely, 'forced bars'. They are two to five times longer than migrating bars (Olesen, 1984; Crosato *et al.*, 2010) and offer an explanation for overdeepening or extra scouring along the outer bank of river bends (Struiksma *et al.*, 1985; Parker and Johanneson, 1989). Both special cases assume a constant discharge. Tubino (1991) extended the theory for bar amplitude growth by Colombini *et al.* (1987) to situations with small variations in discharge.

Non-migrating bars without spatial amplitude gradients at marginal stability (i.e. temporal growth rate equal to zero) arise as a subset of both the migrating bars of Blondeaux and Seminara (1985) and the non-migrating bars of Struiksma *et al.* (1985). This subset represents resonance (Blondeaux and Seminara, 1985; Parker and Johanneson, 1989) and occurs at a specific width-to-depth ratio for given basic-state parameters. Non-migrating bars induced by a local geometrical forcing occur only downstream of the forcing if the width-to-depth ratio is smaller than the value of resonance, but also upstream if the width-to-depth ratio is larger (Zolezzi and Seminara, 2001; Zolezzi *et al.*, 2005; Mosselman *et al.*, 2006).

Migrating alternate bars do occur in laboratory experiments, despite the usual forcing of transversely uniform entrance conditions that violate Blondeaux and Seminara's condition of no influences from the boundaries. Non-migrating alternate bars forced by a local geometrical forcing have been reproduced in laboratory flumes as well, with quasi-equilibrium bed topographies that appear to have more or less the same wavelength and spatial damping as the non-migrating bar pattern formed initially from a flat bed (Struiksma *et al.*, 1985). None of the special theoretical cases of migrating and non-migrating alternate bars arise in real rivers in their pure theoretical forms, but the special cases can serve as approximations of the alternate bars actually occurring. Migrating and non-migrating bars may coexist (Lanzoni, 2000), but non-migrating bars suppress migrating bars (Seminara and Tubino, 1989; Tubino and Seminara, 1990; Lisle *et al.*, 1991). Moreover, long-duration laboratory experiments by Crosato *et al.* (2011) show migrating bars to be a transient feature that eventually develops into non-migrating bars if the discharge remains constant. Non-migrating alternate bars can hence be expected to be much more common in real rivers than migrating alternate bars. The possibility remains, however, that migrating bars are generated episodically if the discharge varies. We investigate this possibility in particular in the present study paying particular attention to the effects of discharge variations, channel geometry and superimposed dunes. The influence of these factors on alternate bar dynamics are of key importance and remain unexplained according to several studies (Lanzoni, 2000; Tubino, 1991). In particular, we seek to see if field measurements performed in a real channel during floods can enrich the theories by detailing the role of local processes and by giving some answers to the following questions: (i) Can discharge variations and specific flow conditions generate new migrating alternate bars from time to time? (ii) What is the effect of non-uniformities in channel width on alternate bars? (iii) How do superimposed dunes affect the migration of alternate bars? We base our study on a detailed data set covering multiple floods and 13 years of intensive field measurements performed in a sandy-gravel secondary channel of the Loire characterized by high and varying (spatially and temporally) width-to-depth ratios, β, and by the occurrence of both migrating and non-migrating alternate bars with superimposed dunes (Rodrigues *et al.*, 2012).

River Presentation and Study Site

Loire River setting

The Loire is the longest river in France and drains a catchment area of 117,000 km^2. At Angers (875 km from the sources), the river has an anabranched pattern (Figure 1) with large islands (Babonaux, 1970; Brossé, 1982; Latapie *et al.*, 2009). For bankfull discharges, width-to-depth ratios (β) of the river channels range between 50 to 400 (Latapie, 2014).

Along the whole river, and particularly downstream of the confluence with the Vienne (815 km from the sources of the Loire), the combined effect of groynes (built in nineteenth and twentieth century) and intense sediment extraction between 1950 and 1995 caused a severe incision of the main branch of the river. This incision led to the disconnection of secondary channels, their rapid colonization by woody vegetation and sediment aggradation (Rodrigues *et al.*, 2006a; Rodrigues *et al.*, 2007), which reduced flow capacity and increased the risk of flooding. Between two flood events, the secondary branches are disconnected from the main channel.

Site description, hydrology and hydraulics

The study site of Ingrandes is located in the lower reaches of the Loire, approximately 30 km downstream of Angers (47° 28′ 32" north, 0° 32′ 64" west). The bedrock (Devonian and Carboniferous conglomerates) present on the right bank deflects the river course towards the south-east. The embanked bed is confined between navigation groynes (Figure 1) and the average slope is *c.* 0.00025 m m^{-1}. The channel splits into two branches, separated by a vegetated and consolidated island. The morphological setting of the bifurcation is asymmetrical: the northern branch, which corresponds to the incised main channel, is narrower and lower [*c.* 4.5 m above sea level (a.s.l.)] than the secondary channel (*c.* 8 m a.s.l.) located on the left bank. The setting of the bifurcation is unusual compared to other systems (Zolezzi *et al.*, 2006; Bertoldi and Tubino, 2007; Kleinhans *et al.*, 2008) and can be explained by anthropogenic modifications in the nineteenth century. At the Montjean-sur-Loire gauging station (6 km upstream), the discharge is 850 m^3 s^{-1} on average and approximately 3200 m^3 s^{-1} for the two-year flood.

The secondary channel is 3070 m long and the bed material is composed of a mixture of siliceous sand and gravels (De Linares and Belleudy, 2007). Its width is 290 m on average but varies locally between 320 and 260 m. In the central part of the channel, where a change in bank orientation is noted, the section is narrower. Just upstream of this point the section is wide. Groynes located upstream of the secondary channel could explain the approximately 45° angle of the bifurcation of the channels, the significant degree of disconnection (3 m high on average), and the presence of large sand bars in this area. Remnants of groynes are also present in the secondary channel (in both the upstream and downstream parts) and influence sedimentological processes in this branch. Most of the banks in the secondary channel have been rip-rapped to protect the island and the dike.

Between 2002 and 2003, two artificial sills were constructed in the main channel (Figure 1) to increase the water level

Figure 1. Location of the Ingrandes study site and close-up showing the bed elevation of the channels. (A) White lines represent surveyed cross-sections and longitudinal tracks (LP1 to LP5). Scour chain transects are shown in black (T1 to T9). (B) Aerial photograph of the study site taken in summer 2009. Bars are numbered within circles (source: DREAL Centre). (C) Map of 1850 of the Loire River near Ingrandes (the bars were already present before the incision of the main channel which occurred since the 1950s). Courtesy of DREAL Centre. This figure is available in colour online at wileyonlinelibrary.com/journal/espl

during low flows (see Rodrigues *et al.*, 2006b, for details). The secondary channel is inundated at a discharge of $450\,m^3\,s^{-1}$ at the gauging station of Montjean-sur-Loire (De Linares, 2007) and reaches its bankfull discharge at $4000\,m^3\,s^{-1}$.

The sills are located downstream of the bifurcation (at the site of former groynes). The main objective was to restore the pre-incision state of the main channel, enhancing the inflow into the disconnected secondary channel during low flows. At the same time, both the inundation duration and the discharges of the secondary channel increased, restoring the flow balance between the two channels during low flows. For total discharges ranging between 700 and $1200\,m^3\,s^{-1}$, discharges recorded in the main channel after the works are $100\,m^3\,s^{-1}$ lower than those measured before the construction of the sills (Figure 2).

As shown in Figure 2, the sills seem to have less effect on discharges above $1000\,m^3\,s^{-1}$ in both branches of the river. No change was observed on the bars present in the secondary channel after the engineering works.

Between 1997 and 2006, nine significant floods and several small events occurred at the study site (Figure 3). Only six floods exceeded $3200\,m^3\,s^{-1}$ (two-year flood), and most of these inundated the secondary channel for many months. The floods of 2001 and 2004, which were investigated in detail, correspond to four- and five-year floods, respectively. Figure 3 shows that all the floods, except the very small ones, were characterized by multiple peaks indicating sudden increases and decreases in discharge.

Materials and Methods

To reach our research objectives, several methods were combined. Bathymetrical surveys, scour chains and stratigraphical observations were used to analyse the bar dynamics, to assess the active-layer thickness available for the development of secondary dunes and to document internal bar structure, respectively. Flow dynamics were assessed from field measurements, gauging station records and one-dimensional (1D) numerical modelling to analyse the key indicators of bar dynamics and sediment transport (e.g. width-to-depth ratio, discharge variations, Shields parameter).

Topographical and bathymetrical surveys

Changes in bed topography in the secondary channel were documented between 1997 and 2005 (Figures 1 and 3) by surveys using a single-beam echosounder (Atlas DESO 22, Atlas Elektronik, Germany) coupled to a differential global positioning system (DGPS) (Trimble 4700, Trimble, USA). A total of 64 cross-sections (see Figure 1 for location), spaced 45 m apart on average (i.e. 33 cross-sections per bar wavelength), was measured during each survey. Fourteen surveys were carried out during the study period for discharges ranging from $155\,m^3\,s^{-1}$ to $4760\,m^3\,s^{-1}$ at the gauging station of Montjean (Figure 3), mostly during floods and in some cases (namely surveys D to G and J to M, Figure 3) at different discharges within the same flood event. During the summer, while the secondary channel was dry, topographical points were measured using the DGPS mounted on a quad bike (surveys E and B). Points were measured every 10 m, excluding inundated pools and banks. Two additional surveys were done recently (O and P) to detail the morphology of the bars during low flows and floods, respectively. The survey O combines aerial LiDAR (light detection and ranging) data from September 2009 with multibeam echosoundings (Seabat 8101 Reson) carried out on 15 February 2010 (data source: Voies Navigables de France). Survey P was performed on 20 February 2013 using a multibeam echosounder (data source: GIP Loire Estuaire) for a discharge equal to $2080\,m^3\,s^{-1}$ at Montjean-sur-Loire gauging station.

Digital elevation models (DEMs) were constructed using the TINs (triangular irregular networks) method which has been demonstrated to be a reliable tool to describe the morphology of alluvial bars (Heritage *et al.*, 2009; Fuller and Hutchinson, 2007; Moore *et al.*, 1991). DEMs were compared to obtain sediment budgets using the three-dimensional (3D) Analyst extension of ArcGis 9 and sediment balance maps.

In 2001 (surveys C to G), five longitudinal tracks almost parallel to the channel banks were surveyed to analyse the migration of bars and dunes during a single flood event using the dune-tracking method (Peters, 1971, 1978; Ten Brinke *et al.*, 1999; Wilbers and Ten Brinke, 2003).

Dune sizes were estimated using the Bedform Tracking Tool Matlab code which is based on a zero-crossing method (Van der Mark *et al.*, 2008). The dune height (H_d) is taken as the difference of elevation between a crest and the downstream trough and the dune length (L) is defined as the horizontal distance between two consecutives troughs. Unfortunately, bedload transport rates could not be derived from dune tracking, because the time periods between two consecutive surveys were too long for determining dune celerities.

To estimate the influence of dune morphology on flow resistance and bar dynamics during the flood of 2001, an average value of the dune roughness parameter was calculated for each bar and for each longitudinal track (LP1 to LP5) using a relation proposed by van Rijn (1984, 1993):

$$k_{\text{dunes}} = 1.1\gamma H_d\left(1 - \exp\frac{-25H_d}{L}\right)$$

where H_d is the dune height, L the dune length, and γ is the dune shape factor taken here as equal to 0.7 since the lee slopes of the

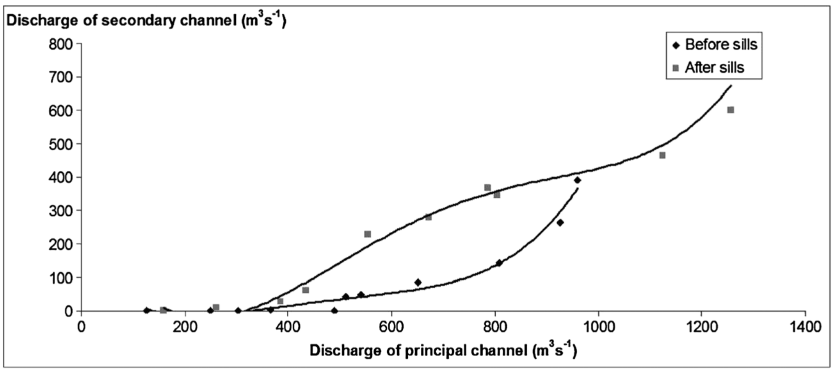

Figure 2. Discharge distribution in the main and secondary channels before and after construction of the sills (data from DREAL Pays de la Loire).

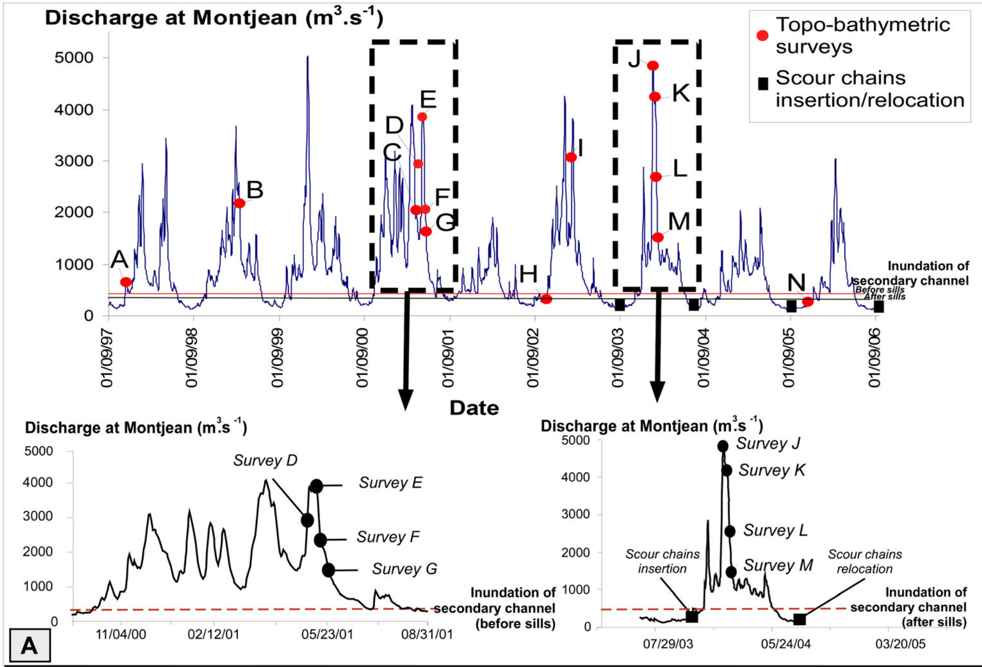

B

Survey	Date	Survey type	Discharge of main channel ($m^3.s^{-1}$)	Average depth (m)	Average water slope ($m.m^{-1}$)	Average bed shear stress ($N.m^{-2}$)
A	11-15-1997	Terrestrial	645	1.0	0.00034	3.3
B	3-15-1999	Echosounding	2170	3.0	0.00027	7.9
C	4-11-2001	Echosounding	2030	2.8	0.00028	7.8
D	5-03-2001	Echosounding	3200	4.1	0.00023	9.4
E	5-10-2001	Echosounding	3840	4.5	0.00023	10.5
F	5-17-2001	Echosounding	2140	3.0	0.00027	7.9
G	5-23-2001	Echosounding	1630	2.3	0.00028	6.4
H	10-21-2002	Terrestrial	315	0	Dry channel	0
I	2-06-2003	Echosounding	3070	3.9	0.00024	9.2
J	1-20-2004	Echosounding	4760	5.1	0.00025	12.4
K	1-28-2004	Echosounding	4200	4.9	0.00024	11.6
L	2-04-2004	Echosounding	2680	3.5	0.00026	9.1
M	2-11-2004	Echosounding	1500	2.3	0.00031	7.0
N	11-15-2005	Terrestrial	155	0	Dry channel	0
0	Sept. 2009 & Feb.2010	LiDar/Multib. echosounding	No data	No data	No data	No data
P	2-20-2013	Multib.echosounding	2080	No data	No data	No data

Figure 3. Hydrographs at Montjean-sur-Loire gauging station (6 km upstream), associated surveys carried out during the study period and average hydraulic characteristics of the secondary channel. In 2009 and 2013 two surveys combining aerial LiDAR data and multibeam echosoundings were performed; they are not mentioned in this figure.

dunes in the channel were observed to be less than the angle of repose (see van Rijn 1993; Paarlberg *et al.*, 2010).

Scour chains and stratigraphy of deposits

Between 2003 and 2006, the active layer associated with the migration of alternate bars and dunes in the secondary channel during floods was studied using the scour chain method (Hassan, 1990; Laronne *et al.*, 1994; Hassan *et al.*, 1999; Rodrigues *et al.*, 2012). A total of 99 metal-link chains was inserted vertically, anchored into the stream bed, and located along *x*, *y*, *z* axes using a DGPS. Scour chains were inserted at nine cross-sections (T1 to T9) identified during bathymetric surveys. At each scour chain location, surface bed sediments were sampled for grain-size analysis during insertion and location phases. The scour chains were located after the floods by digging the channel bed using the DGPS and a metal detector. The scour and fill depths of bed material during floods were determined by measuring the length of the chain above the elbow (maximum scour depth) and the distance between the elbow and the post-flood bed level (subsequent sediment deposition). Grain-size analyses were performed on 133 sediment samples taken at each scour chain location using standard Ro-Tap dry sieving and laser counting methods.

Internal bedform structures were analysed by trenching down to the water table during low-flow periods when the scour chains were located. Trenches were dug at scour chain locations chosen for the value of scour and fill depths and the spatial distribution of large bedforms. Flood-related sedimentary units were identified in the sequence (Allen, 1984; Miall, 1996; Bridge, 2003), described in detail on two faces of each pit (longitudinal and transverse depending on the main flow direction), and their thickness was measured. Scaled photographs were taken in order to compare the position of each unit with the bed surface documented by bathymetrical surveys during floods (Rodrigues *et al.*, 2012).

Hydraulics

The flow dynamics were assessed from measurements of water levels and flow velocities. DREAL Pays de la Loire has been recording water levels since 1997. They also measured flow velocities in the secondary channel at cross-section T4 between 2002 and 2012 using an Acoustic Doppler Profiler (RDI Rio Grande, 1200 kHz). These measurements were carried out to detail the flow dynamics at the start of flooding of the secondary channel.

Both water level and flow velocity measurements were used to set up a hydrodynamic model of the Loire between Angers and Nantes in 2012. We used the HydraRiv software (Hydra, 2010), which allows combining various schematizations, ranging from 1D to fully two-dimensional (2D), in a single model. The 1D component is applied to the main stream and adjacent plains whereas the 2D part is used to model flows in the groyne fields. Both parts are based on the Saint-Venant equations that are solved using an implicit finite-volume method.

Results obtained with this model were compared to field measurements given by DREAL Pays de Loire and to the results of a local 2D model previously developed for the study site by De Linares (2007).

Results

Hydraulic geometry and bar regime

Flow conditions in the secondary channel

Table I and Figure 4 show that mean flow velocities ranged between 0.6 and 0.9 $m\,s^{-1}$ when discharges at Montjean-sur-Loire gauging station were equal to 1110 and 1890 $m^3\,s^{-1}$, respectively.

For the same overall flow conditions, corresponding to the first stage of inundation of the channel, the discharge entering the secondary channel represented 24 and 35% of the total discharge, respectively. In other words, a small variation of discharge in the main channel can be associated with a significant variation of the flow dynamics in the secondary channel.

Figure 4A shows that the width-to-depth ratio (β) at cross-section T4, measured in the field and calculated using the 1D model, ranges between 55 and 230. The decrease of the width-to-depth ratio (β) with increasing discharges is significant until the discharge flowing in the secondary channel is almost 800 $m^3\,s^{-1}$ (*c.* 1900 $m^3\,s^{-1}$ at Montjean-sur-Loire). For higher discharges, the width-to-depth ratio (β) decreases less rapidly. The decrease of the width-to-depth ratio (β) is accompanied by an increase of average flow velocity and total bed shear stress. Values of the Shields mobility parameter related to skin friction range between 0.05 and 0.15 (Figure 4B). This point highlights the high mobility of the sediments present in the secondary channel, even during low flows.

As shown by Figure 4A, the average flow velocities calculated using the model are lower than those measured during the field surveys for secondary-channel discharges ranging from 261 to 729 $m^3\,s^{-1}$ (corresponding to discharges of 1110 and 1890 $m^3\,s^{-1}$ in the main channel, respectively). The decreasing trend of the relative roughness with increasing discharges is somehow similar to the decrease in width-to-depth ratio (β).

Width-to depth ratio (β) for unsteady flow and bar regime

Figure 5 shows width-to-depth ratio (β) values ranging from 43 to 252 for discharge conditions at Montjean-sur-Loire ranging from 645 to 4760 $m^3\,s^{-1}$. The variability of the width-to-depth ratio (β) values is influenced by the longitudinal variation of the channel width. For instance, large values of β are visible between cross-sections T1 and T2, between T3 and T4 and downstream of T8.

Channel bed evolution and morphodynamics of bars

Bar morphology and dynamics

Large-amplitude bed waves (Figure 6) with an average height of 1.5 m were found alternating on both sides of the secondary channel. Their wavelength is equal to 1500 m. Most of these bars are asymmetrical in along-stream direction, typically with a diagonal lobate avalanche face upstream of a scour pool associated with a lateral pool.

The top of bars is visible on the DEM at an average elevation of 9.5 m a.s.l. (Figures 6 and 7). In the upstream part of the

Table I. Flow conditions for cross-section T4 between 2002 and 2012.

Date	3 November 2002	14 January 2003	29 January 2003	8 December 2003	3 May 2005	11 April 2006	31 January 2007	11 May 2012
Total discharge at Montjean -sur-Loire ($m^3\,s^{-1}$)	1110	1820	1530	1890	1200	1490	1180	1250
Discharge in secondary channel ($m^3\,s^{-1}$)	261	603	466	729	438	541	416	472
Percentage of total discharge (%)	24	33	30	39	36	36	35	38
Section width (m)	275	290	283	283	282	285	284	274
Wetted area (m^2)	443	748	612	813	572	629	514	555
Width-to-height ratio (–)	172	112	131	99	139	129	157	126
Average flow velocity u ($m\,s^{-1}$)	0.62	0.81	0.77	0.91	0.80	0.88	0.84	0.86
Average water depth H (m)	1.60	2.58	2.16	2.87	2.03	2.21	1.81	2.17
Froude number Fr (–)	0.16	0.16	0.17	0.17	0.18	0.19	0.20	0.19
Chézy skin friction factor C′ ($m^{0.5}\,s^{-1}$)	68.6	72.3	71.0	73.2	70.5	71.1	69.6	71.0
Specific stream power ω ($W\,m^{-2}$)	2.3	5.1	4.0	6.3	3.8	4.7	3.6	4.2
Bed shear stress τ ($N\,m^{-2}$)	3.9	6.3	5.3	7.0	5.0	5.4	4.4	5.3
Grain shear stress τ′ ($N\,m^{-2}$)	0.81	1.23	1.16	1.52	1.27	1.51	1.45	1.43
Shields mobility parameter (skin friction) θ′ (–)	0.06	0.09	0.09	0.11	0.09	0.11	0.11	0.11
D_{90} /water depth (H)	0,0019	0,0011	0,0014	0,0010	0,0015	0,0013	0,0016	0,0014

$Fr = u/\sqrt{gH}$ where g is the acceleration due to gravity, H is the mean flow depth, $C' = 5.75\sqrt{g}\,\log\left(\frac{12H}{k_s}\right)$ with $k_s = D_{90}$, $\omega = \frac{\rho g Q S}{W}$ where ρ is the density of water, Q is the discharge in the secondary channel, S is the water surface slope, taken here as constant (0.00025), W is the width of the channel, $\tau = \rho g H S$, $\tau' = \rho g\left(\frac{u}{C'}\right)^2$ and $\theta' = \frac{u^2}{C'^2(s-1)D_{50}}$ where s is the relative submerged sediment mass density (equal here to 1.65)

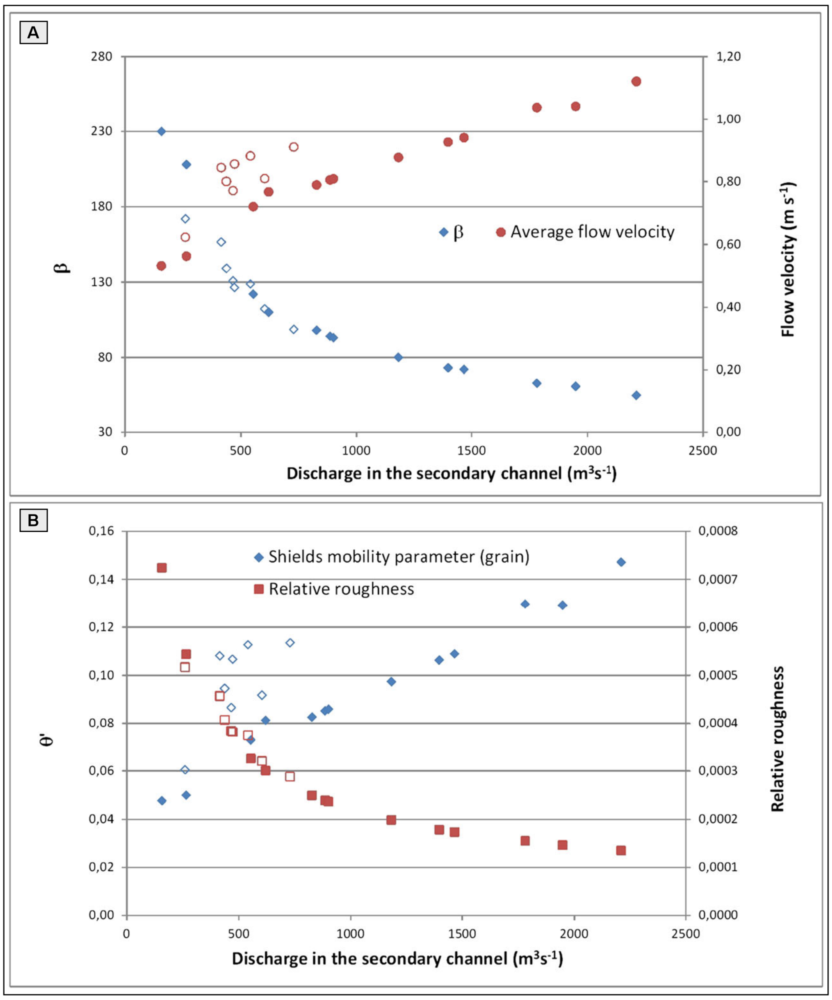

Figure 4. Measured (open symbols) and predicted (closed symbols) values at cross-section T4 of (A) width-to depth ratio (β) and flow velocity, (B) Shields mobility parameter (related to grain friction) and relative roughness (D_{50}/flow depth) plotted versus the discharge in the secondary channel. This figure is available in colour online at wileyonlinelibrary.com/journal/espl

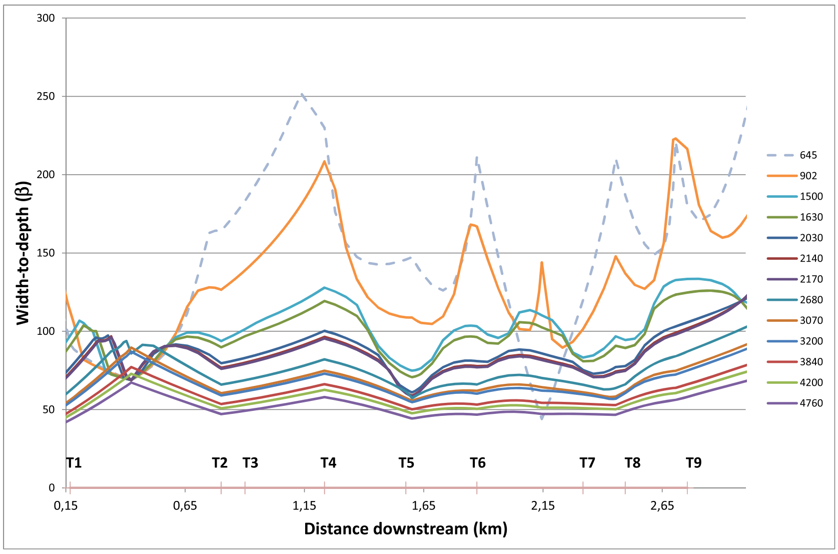

Figure 5. Width-to-depth ratio (β) of the secondary channel calculated for various flow conditions using the Hydrariv model. Cross-sections T1 to T9 are mentioned on the x-axis. The dashed curve (645 $m^3 s^{-1}$) corresponds to the first stage of channel inundation which explains the unrealistic pattern of this curve. Flow is from left to right. This figure is available in colour online at wileyonlinelibrary.com/journal/espl

channel (from T1 to T5) the non-migrating bars 1 and 2 are present. Bar 1 is due to the curve of the Loire upstream of the inlet of the secondary channel and to the presence of groynes upstream of the study site (see Figure 1 for location). Bar 2 can be considered as a non-migrating bar located in a wider part of the channel delimited downstream by a narrower part of the channel. The planform and location of this bar evolve between the banks according to discharge conditions: significant

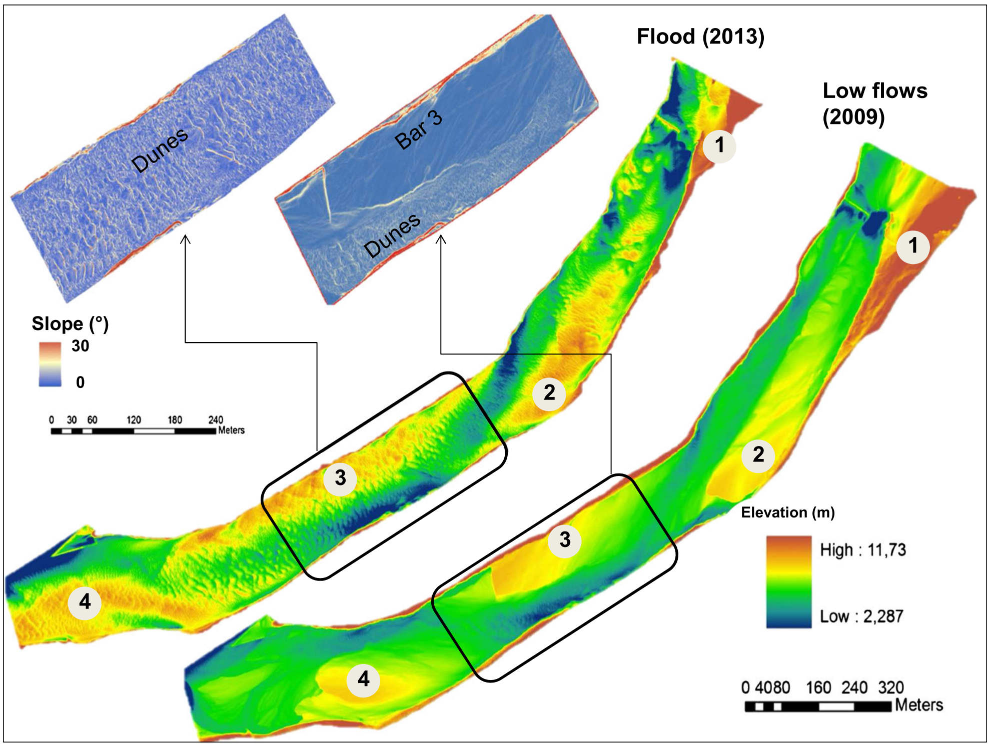

Figure 6. Bars present in the secondary channel of the study site of Ingrandes. Digital elevation models (DEMs) obtained for low flows of year 2009 (by combining aerial LiDAR data and multibeam echosoundings) and a flood event (year 2013, multibeam echosoundings). Slope maps focused on bar 3 are also presented for both flow conditions. This figure is available in colour online at wileyonlinelibrary.com/journal/espl

Figure 7. Aerial photograph of the study site (source: GIP Loire Estuaire) showing alternate bars in the secondary channel (A). Lateral pool and thalweg (low-flow period) separating two alternate bars in a single-row configuration (B). Silt and mud deposits downstream of the slipface of an alternate bar (C). Slipface of an alternate bar (1.5 m high) during low-flow period (D). Note the significant angle of the front (near angle of repose). Flow is from left to right. (E),(F) Upstream and along-stream view of sand and gravel cross-bedding corresponding to dunes overlaid by small-scale cross-stratified sandy ripples. Top of high-angle gravelly foreset bed (35°) is truncated by strongly concave laminae. This figure is available in colour online at wileyonlinelibrary.com/journal/espl

aggradation occurs during high water levels and sediment reworking during low flows. Numerous rills and small deltas in the bar-tail region contribute to a lateral extension of the bar at low flows. The second part of the channel, located downstream of the area with a change in bank orientation and associated to a chute, is characterized by bars 3 and 4. The bar mode is equal to one. The formation of bar 3 always occurs near the earlier-mentioned chute and a geometrical discontinuity of the channel banks. In this part of the channel, another chute associated with a change in bankline orientation is visible between T8 and T9 (see Figure 1).

Although the bar surfaces are relatively smooth when the water leaves the channel (Figure 6, low flows 2009), some slope breaks are visible. Most of these slope breaks correspond to migration fronts of large dunes or to rills. Superimposed dunes were always observed on the back of macroforms during floods and were reworked during low flows. During low flows, dunes present in the thalweg are constrained by bars and adopt a zigzag pattern.

Armour layers were often identified at the upstream part of bars, on riffles, and more rarely on rills on the back of large bars. This distribution is reminiscent of the findings of Lisle *et al.* (1991, 1993).

All the bars are characterized by a well-developed front located near the bank which is less visible in the inner part of the channel. The general slope direction of the back of bars (Figure 6) depends on the location of the bars in the channel.

Data acquired between 1997 and 2005 (Figure 8) suggest that no significant change in the average general elevation of the bars occurred during their migration. Moreover, they suggest that bar formation is strongly influenced by the morphological configuration of the channel. For instance, the migration of bar 2 is influenced by the variation in width of the channel and the presence of the remnants of the groynes near the entrance of the channel. Upstream of the narrower channel section the migration is mostly lateral. Its spreading downstream is made impossible by the narrower cross-section.

The different orientation of the banks between transects T3 and T5 induced the development of a chute which is visible on almost all the DEMs shown in Figure 8. This chute separates bars 2 and 3 in this low-amplitude meandering part of the channel. During floods, bar 3 can elongate downstream and divide into two smaller bars, 3a and 3b [see surveys A ($645\,m^3\,s^{-1}$) and J ($4760\,m^3\,s^{-1}$) to M ($1500\,m^3\,s^{-1}$), Figure 8). During this study, this phenomenon (which will be discussed later) occurred twice (surveys A and N). The downstream part

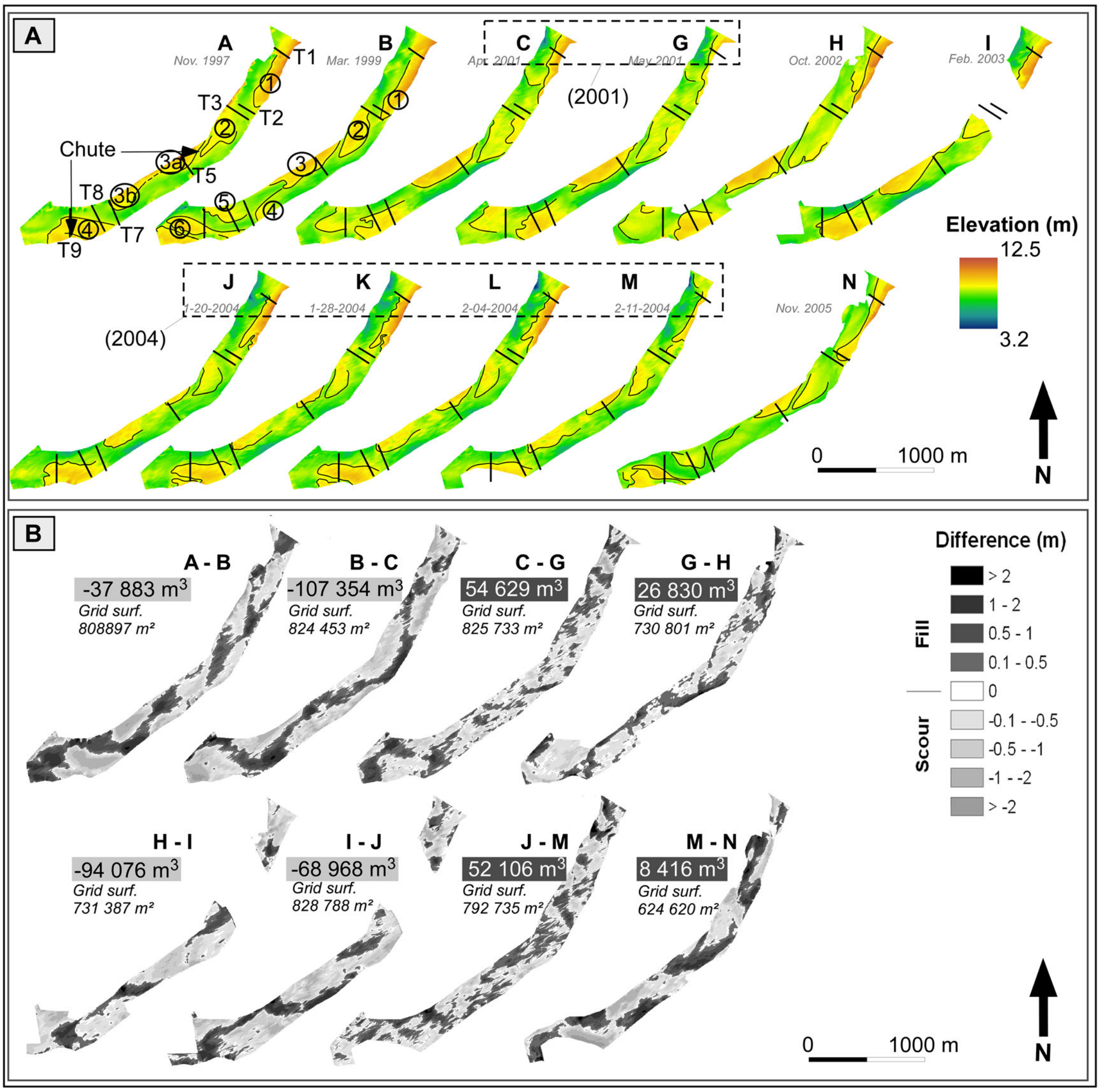

Figure 8. Digital elevation models (A) and sediment balance maps (B) detailing sediment budgets and area of calculation obtained by bathymetric surveys (bold letters) between 1997 and 2005 (see Figure 1 for discharge conditions for each survey). Dashed lines correspond to surveys conducted during a single flood event. Numbers in circles refer to bars, and T1 to T9 correspond to scour chain transects. Data of surveys O and P were excluded from this analysis. This figure is available in colour online at wileyonlinelibrary.com/journal/espl

of bar 3 has migrated downstream since 1999, while another bar appeared in the same place during the flood of 2004 [surveys J (4760 $m^3 s^{-1}$) to M (1500 $m^3 s^{-1}$), Figure 8). The configuration of the bars described here is similar to the one documented during survey A (645 $m^3 s^{-1}$). The second chute, located at the downstream end of the channel, may also modify the local flow and sediment transport conditions, explaining both the coalescence and the reworking of bar sediments in this area. On DEMs A, B and C (Figure 8), the initiation of bar 4 is visible at the left bank of the secondary channel, between bars 3a and 3b. On DEM C this bar is well-developed, increasing in size as bar 3a becomes larger. Sediment balance maps confirm the migration of the bars; the pattern of scour and fill areas between two surveys is clearly associated with the stoss side and progradation fronts of the bars, respectively. On most sediment balance maps this pattern is relatively diagonal in relation to the orientation of banks. This shows that the downstream migration of bars is characterized by a lateral spreading over the area, including the space separating two bars and the lateral pool associated with each bar (Church and Rice, 2009). There is no evidence of a direct link between sediment budgets and discharge during floods, but sediment deposition is associated with large-magnitude floods followed by low-magnitude events. Conversely, scouring is mainly associated with low-magnitude floods.

Once initiated, bars 3, 4 and 5 migrated longitudinally according to a pattern which was more or less the same in the secondary channel between 1997 and 2009. The celerity of their fronts differed according to discharge and to the position in the cross-section (Table II).

Table II shows that the celerity of the bar fronts was variable spatially (i.e. location in the cross-section) and temporally (controlled by discharge variations). Maximum and minimum values recorded were respectively 6.6 and 0.2 m day^{-1}. Table II also shows that the celerity of each bar responded differently to discharge variations during the same flood event (e.g. bars 3 and 5 during the flood of 2001). Bar celerity decreased most of the time substantially during the falling limb of the floods monitored.

Active layer thickness associated with bar migration

Results show that the deepest scour is associated with the flood of 2003 to 2004, apart from cross-sections T7 and T9 where pre-flood deposition of the large alternate bar 4 reduced this trend (Figure 9). In T1, scour depths are less than in the other sections, ranging from 0 to 0.8 m, while fill depth does not exceed 0.7 m. In T5, bar 3 is present on the right side of the channel while the thalweg is on the left. As shown in Figure 9, bed elevation varies less on the right side (except between 2003 and 2004) whereas scour and fill values increase significantly toward the left bank. On T7 the asymmetrical pattern of the sediment budget for the 2003–2004 flood can be explained by the alternate configuration of bars at the beginning of the flood: sediment deposition on the right corresponds to the progradation of the front of the upstream bar while sediment scouring on the left can be explained by erosion on the upstream part of the bar on the left side of the channel. Active layer thickness values are high at T9 compared to the other sections. During the 2003–2004 flood, the bar immediately upstream of T9 prevented erosion in the central part of the channel. This bar extended laterally in the northeast (NE) direction. The DEMs of 2004 and 2005 show that the chute induced significant erosion, as shown by the two scour chains near the left bank. At the same time, the channel bed was subject to intense erosion 150 m from the right bank. This phenomenon can be explained from deflection of the flow by the edge of the bar.

Type of deposits and internal structure of migrating alternate bars in relation to their dynamics

As shown by Figure 10, sediments collected when the channel was disconnected were mainly made of sands (medium, coarse and very coarse) and very fine gravels. The median grain size, D_{50}, ranges between 300 μm and 4165 μm while the grain size not exceeded by 90% of the sediment mass, D_{90}, ranges between 427 μm and 14 998 μm. The sediments of bars are slightly finer than the sediments taken from the lower parts of the channel bed. The sorting of the sediments, defined as the inclusive standard deviation σ proposed by Folk and Ward (1957), is poor ($1 < \sigma < 2$) to very poor ($2 < \sigma < 4$) and increases as the sediments get coarser.

The internal structure of bars consists mainly of relatively simple large-scale sets of planar cross strata of coarse sands and gravels (Figures 7F and 11). This type of internal structure is reminiscent of 'large bar margin slipfaces' indentified firstly by Smith (1974) and afterwards by Lunt and Bridge (2004). This large-scale bedding depends on the migration of superimposed dunes (Reesink and Bridge, 2007; Reesink *et al.*, 2014) and is affected by reactivation surfaces attributed to fluctuations in flow stages (Figure 11, C4).

The thickness of large-scale planar cross tabular sets ranges between 0.1 and 1 m. This thickness frequently decreases upwards. The beds are at an angle of repose or less and are

Table II. Celerity (in m day^{-1}) of the fronts of migrating bars 3 to 5 for floods of 2001 and 2004

	Bar	Survey D–E	Survey E–F	Survey F–G	Distance from right bank (m)
Discharge variation		+640 $m^3 s^{-1}$	−1700 $m^3 s^{-1}$	−510 $m^3 s^{-1}$	
Flood 2001 (maximum discharge 4070 $m^3 s^{-1}$)	3	3.4	2.9	0.3	22
	3	4.5	2.9	No data	52
	4	No data	3,2	No data	256
	5	2.9	0.2	1.7	22
	5	4.3	4.3	5.1	52
Discharge variation	Bar	Survey J–K	Survey K–L	Survey L–M	Distance from right bank (m)
		−560 $m^3 s^{-1}$	−1520 $m^3 s^{-1}$	−1180 $m^3 s^{-1}$	
	3	6.6	1.6	1.5	22
Flood 2004 (maximum discharge 4840 $m^3 s^{-1}$)	3	5.2	3.6	2.5	52
	4	6.1	2.8	2.7	193
	4	6.6	3.7	No data	256

Celerity of bar tail was assessed from topo-bathymetrical surveys D (3200 $m^3 s^{-1}$), E (3840 $m^3 s^{-1}$), F (2140 $m^3 s^{-1}$), G (1630 $m^3 s^{-1}$), J (4760 $m^3 s^{-1}$), K (4200 $m^3 s^{-1}$), L (2680 $m^3 s^{-1}$) and M (1500 $m^3 s^{-1}$) for various distances from the right bank. Unfortunately, it was impossible to measure bar celerity in the central part of the channel. Surveys D and E were performed near the flood peak.

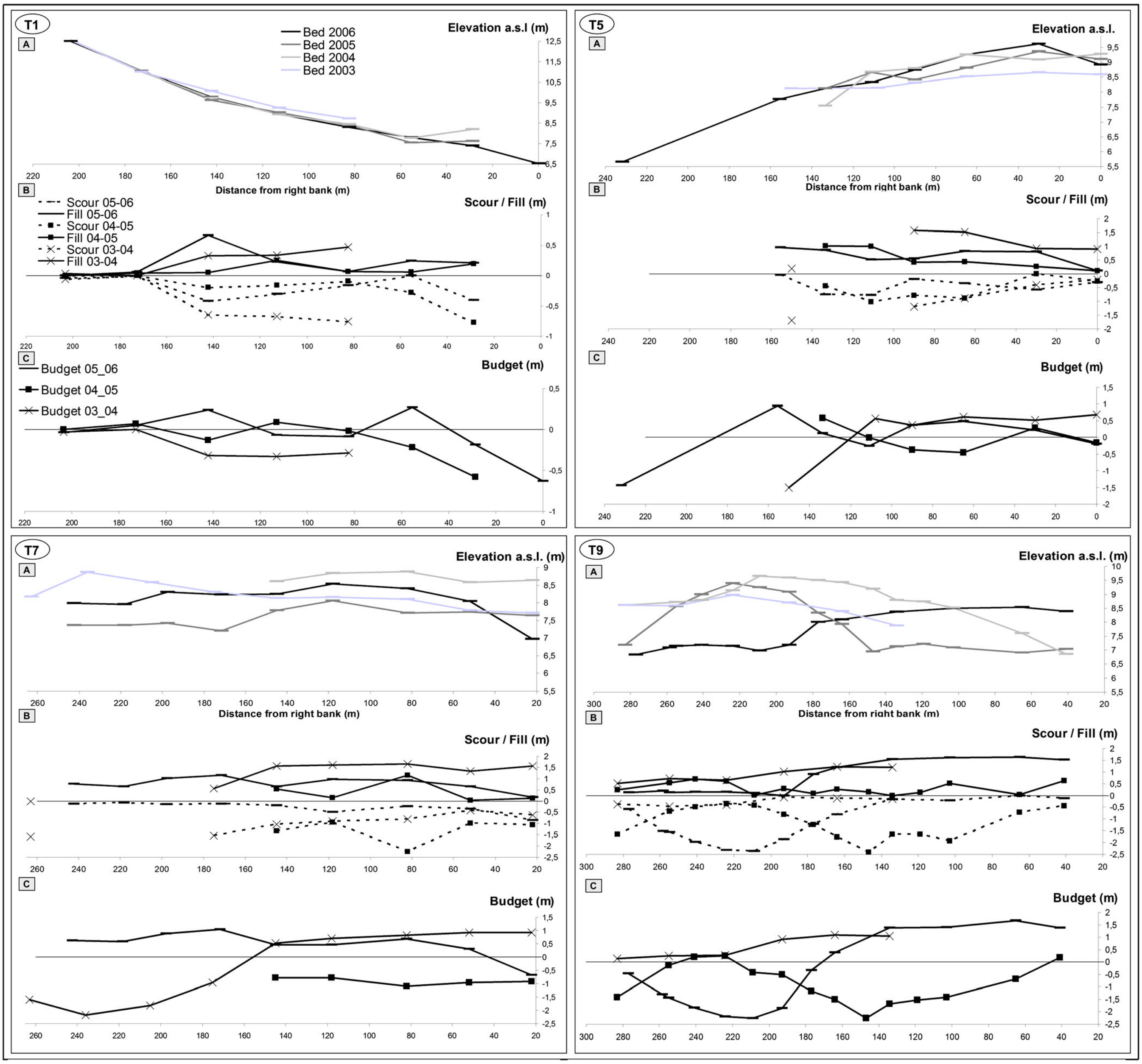

Figure 9. Scour and fill depths obtained for cross-sections T1, T5, T7 and T9 between 2003 and 2006: (A) bed topography during the dry periods; (B) scour and fill depths during flood events; (C) sediment budgets (difference in channel bed topography before and after the floods). See Figure 1 for scour chain insertion and relocation.

characterized by vertical sorting. The direction of steeply dipping sands is variable due to the location of the bar relative to the channel and to its local direction of migration.

Medium-scale cross stratification consists of planar or trough bedding corresponding to the migration of 2D or 3D dunes (Allen, 1984; Ashley, 1990; Miall, 1996). The form of foreset laminae can change from concave to planar following the direction and intensity of the flow. Average coset thickness of 0.1 m implies an average dune height of 0.3 m (Leclair *et al.*, 1997). This is consistent with the height of dunes measured during floods (see following sections).

Small-scale planar cross-sets associated with ripple migration are formed of medium to fine sand and can be preserved as sets interbedded with dunes or bar sediments (Figure 11, C4). Sometimes counter-current ripples occur at the base of the foresets of simple large-scale planar cross strata.

Planar strata are found at the tops of bars. These strata are thought to be linked to sediment reworking during low flows and explain the smoothed aspect of the bar surface.

One-centimetre-thick dark silty and muddy layers (D_{50} equal to 9 μm) were observed at different depths during trenching. They can overlay gravelly deposits corresponding to ponds or to the former thalweg or be interbedded with bar sediments. These beds result from the settling of fine sediments when the channel empties or due to local flow conditions (Ashworth *et al.*, 2000; Best *et al.*, 2003, Rodrigues *et al.*, 2012).

Figure 11 also shows that the preservation of sediments is influenced by the presence of the bar; at C3 and C5, respectively, previously deposited sediments were eroded or protected according to the distance from the avalanche face upstream.

Dynamics of superimposed dunes and bars for unsteady flow conditions

Dune morphology and associated hydraulic roughness

Longitudinal tracks (LP1 to LP5, see Figure 1) carried out for various discharge conditions during the last flood peak of

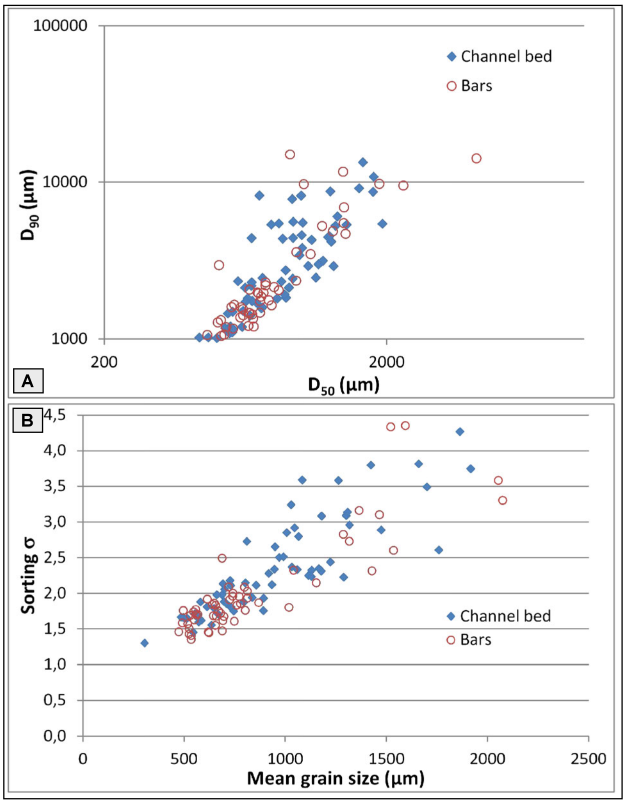

Figure 10. Grain size and sorting of surface sediments present on the bars and on the channel bed between 2003 and 2006. Areas where water was present were excluded from this analysis. This figure is available in colour online at wileyonlinelibrary.com/journal/espl

2001 (surveys C to G) highlighted the migration of bedforms on the bars as well as the increase in bar length (Figure 12). The average height and length of the dunes ranged between 0.05 and 0.7 m and between 2 and 37 m, respectively. The average steepness (H_d/L) of the dunes was equal to 0.023. This value is low in comparison to the minimum value of steepness 0.06 commonly admitted for equilibrium dunes (Carling *et al.*, 2000), which can be attributed to an inadequate sediment supply (Claude *et al.*, 2012) or a depth limitation. Here, the hypothesis of a low sediment supply cannot be retained since the thickness of the active layer of sediments composing the bars is larger than the height of the dunes (Figure 11; and see Villard and Church, 2005; Tuijnder *et al.*, 2009).

As shown by Figure 12A, the height and length of dunes varied during the investigated flood according to a counterclockwise hysteresis. This means that height and length of dunes were higher during the falling limb of the hydrograph than during the rising limb due to time lags in dune development. The increase of dune height and length was often more significant during the rising limb, especially during the high discharges reached between surveys D (3200 $m^3 s^{-1}$) and E (3840 $m^3 s^{-1}$). This trend was observed on each of the bars during the flood event of 2001, irrespective of the location on the bar (see Figure 12). Contrarily, on all bars except the non-migrating bar 2, average dune steepness followed a clockwise hysteresis during the same flood event.

The evolution of the height and length of dunes can be described more precisely according to the flood stage and the bar considered. During the rising limb (i.e. between surveys C and D), Figure 13 shows that the increase in dune length was significant while the increase in height was moderate.

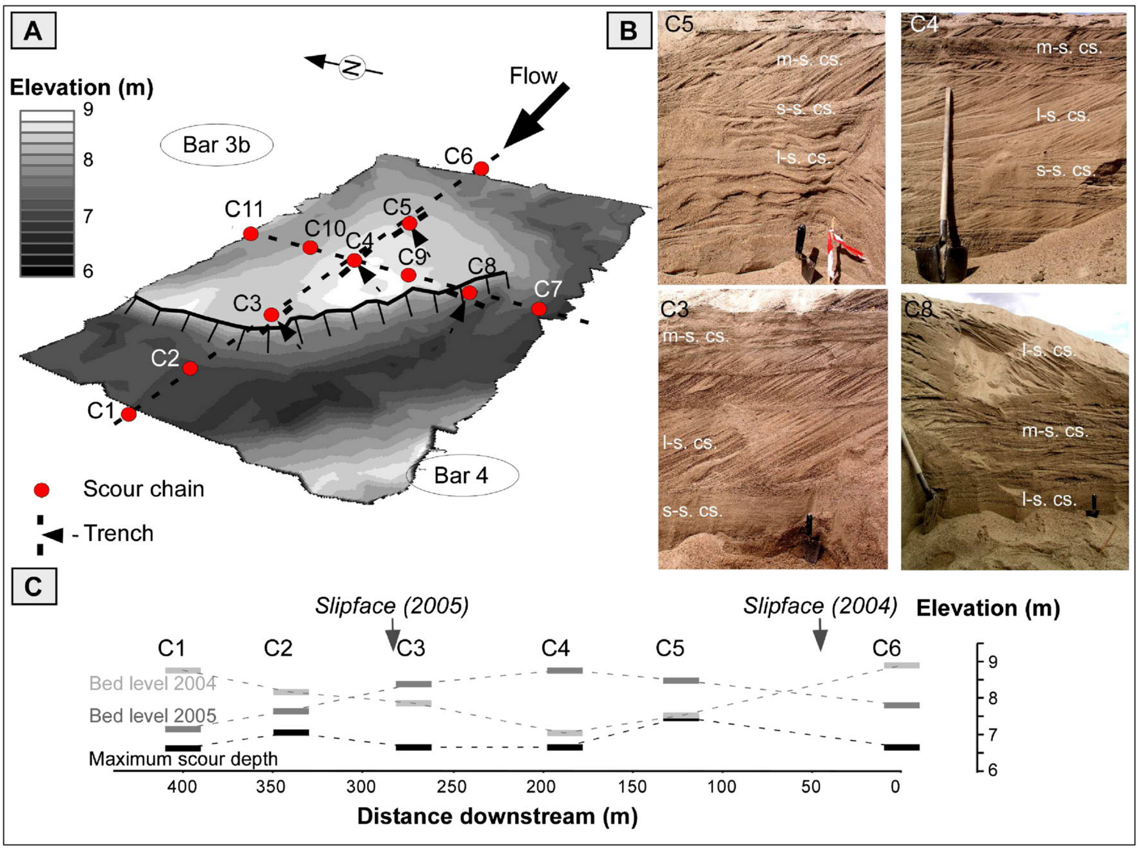

Figure 11. Morphology in 2005 (A), internal structure (B), migration front and associated longitudinal scour and fill depths (C) of bar 3b (see Figure 8 for location) deposited in the downstream part of the channel between 2004 and 2005. Scour chains (e.g. C3) and trenches are located. S-s cs, m-s cs and l-s cs are respectively small-scale, medium-scale and large-scale cross stratification. This figure is available in colour online at wileyonlinelibrary.com/journal/espl

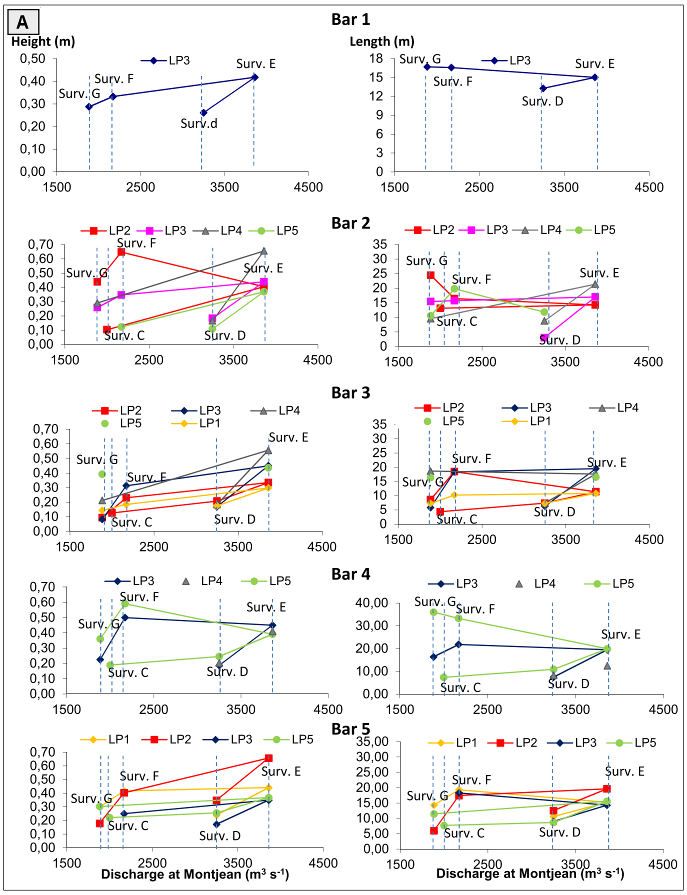

Figure 12. (A) Evolution of dune height and length on bars present in the channel during the flood event of 2001 (surveys C to G). LP1 to LP5 correspond to the bathymetrical longitudinal tracks. (B) Average dune steepness (calculated from the longitudinal tracks LP1 to LP5 present on each bar) plotted versus flow discharge at Montjean-sur-Loire gauging station for bars 2 to 5. Hydraulic roughness of dunes (k_{dunes}) present on the back of alternate bars for surveys C to G. No data available for bar 1 during survey C. This figure is available in colour online at wileyonlinelibrary.com/journal/espl

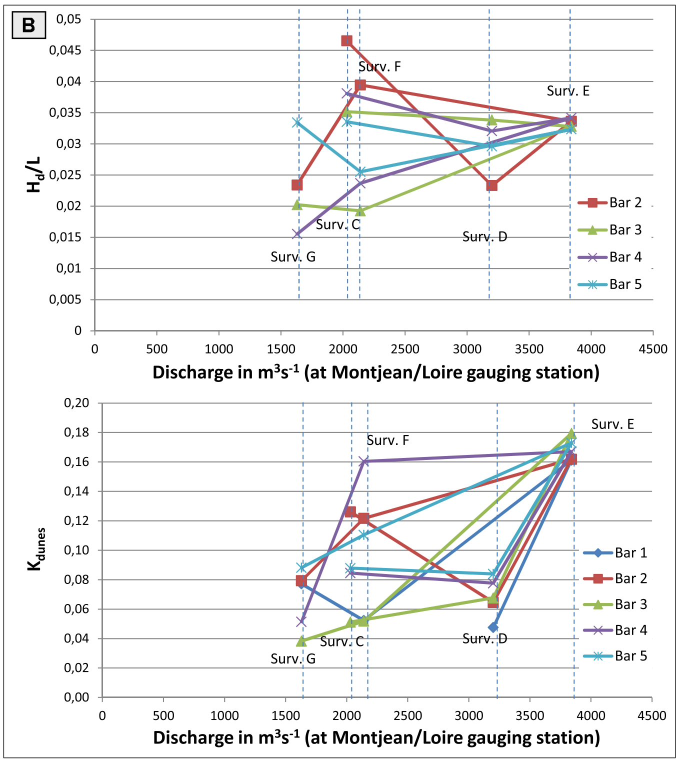

Figure 12. (Continued)

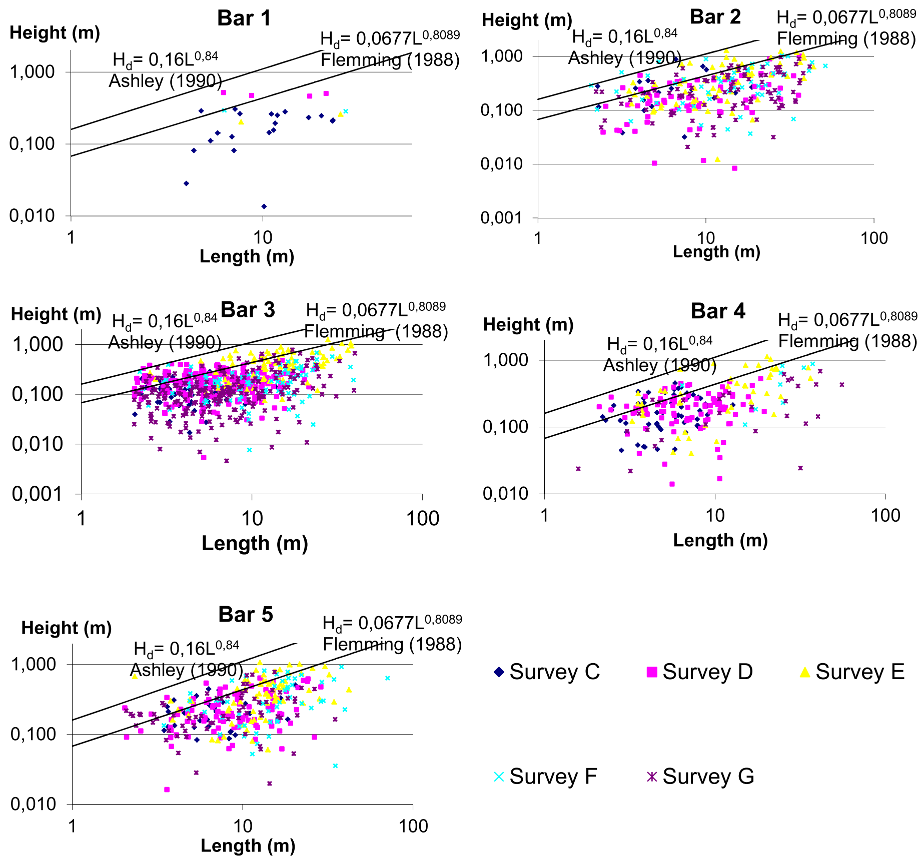

Figure 13. Evolution of average height and length of dunes present on each bar between surveys C and G. See the shifting of the points according to discharge variations. Equations of Flemming (1988) and Ashley (1990) are given as references. This figure is available in colour online at wileyonlinelibrary.com/journal/espl

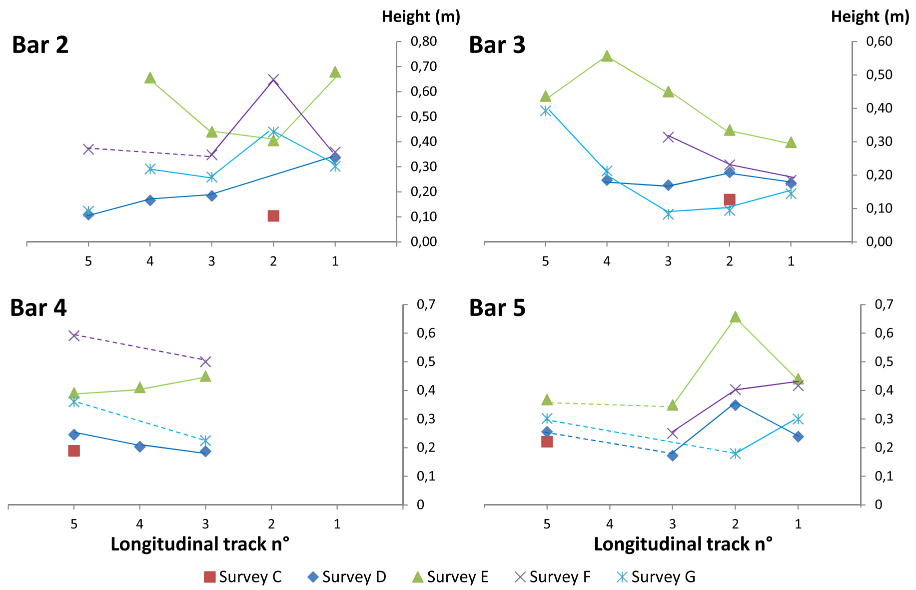

Figure 14. Cross-sectional evolution of average dune height (measured along the longitudinal tracks LP1 to LP5) on bars 2 to 5 between surveys C to G (flood of 2001). Right and left bank are located on the right and on the left of each graph, respectively. Bar 1 was excluded because data were only recorded on LP3. This figure is available in colour online at wileyonlinelibrary.com/journal/espl

During the falling limb of the hydrograph, the morphological response of dunes to discharge variation differed according to the bar considered (see bars 2 to 5 between surveys E and G).

The influence of dunes on flow and sediment transport can be described in terms of hydraulic roughness parameter k_{dunes}. Figure 12B shows that k_{dunes} values on bars were increasing in the downstream direction during surveys D and E. Higher values of k_{dunes} were reached during survey E on all the bars present in the secondary channel. After this survey, values of k_{dunes} remained high on bars 2, 4 and 5. Figure 12B suggests that the dunes exerted a significant influence on flows between surveys E and F.

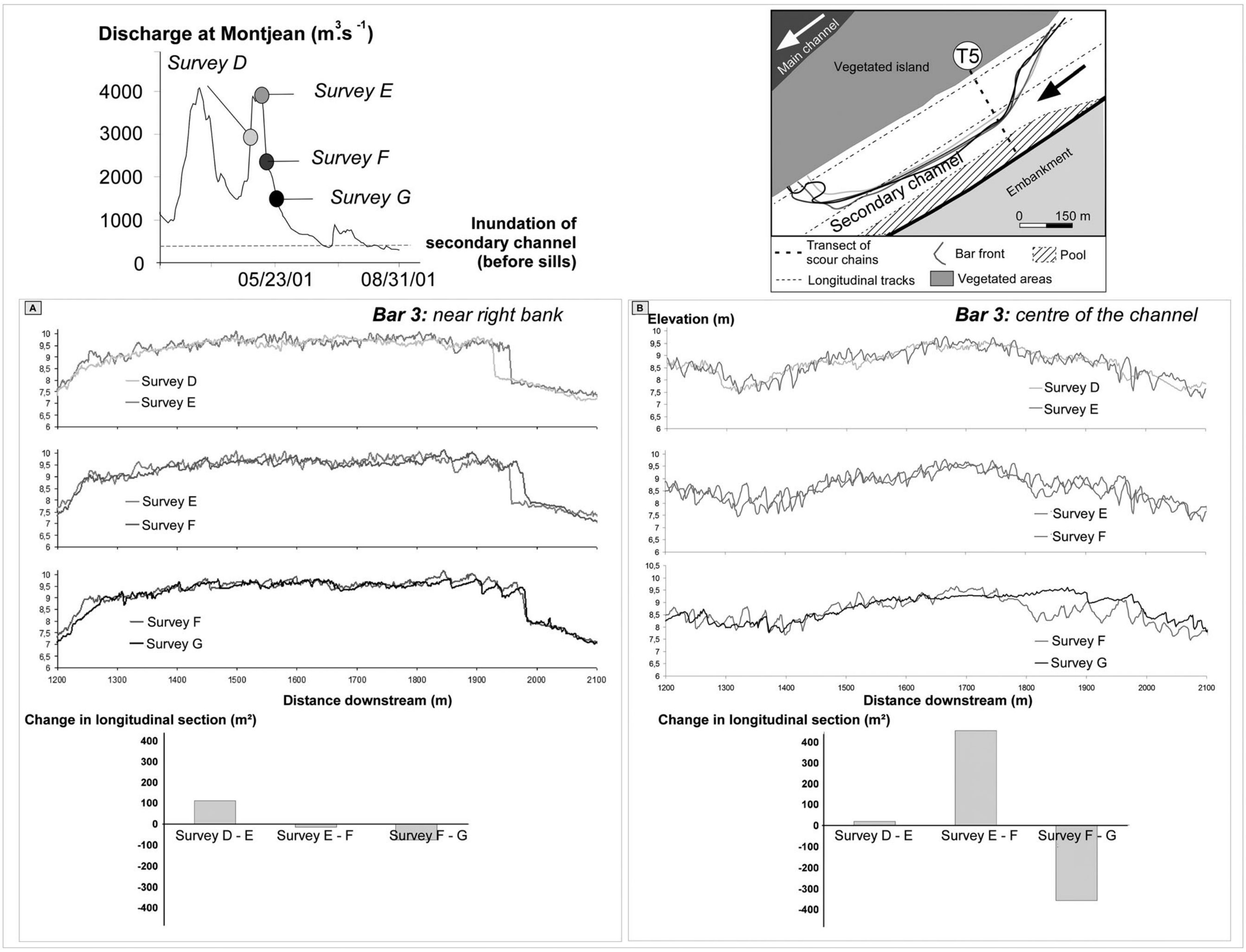

Figure 15. Comparison of longitudinal bathymetrical tracks (LP1 and LP4) performed on bar 3 during the last peak of the 2001 flood for four discharge conditions (D, E, F and G; from light grey to dark grey).

Transverse variability of dune dynamics on bars

Dunes present on bar 3 show a strong correlation between the height of dunes and the distance from the right bank (Figure 14). This can be attributed to the lateral variation of flow depth (Julien and Klaassen, 1995; Yalin, 1977) associated with the transverse slope of bar 3 (Figure 14).

In other words, the increase in dune height is more important for high flow depths.

This transverse variability is clearly visible along the longitudinal tracks (Figure 15). Notably, the bar tail underwent significant reworking during the falling limb of the flood (illustrated by the development of four secondary dunes near the front).

This is not the case in the profile located in the central part of the cross-section where the avalanche face appeared during surveys F ($2140\,m^3\,s^{-1}$) and G ($1630\,m^3\,s^{-1}$). Here erosion could be perceived on the upstream part of the bar and deposition on the downstream part (as described in Ashworth *et al.*, 2000). The resulting smoothing of the bar surface occurred simultaneously with the development of the avalanche face in the central part of the section.

Hence, changes in longitudinal profiles (Figure 15) vary significantly according to profile location and flood stage. Between surveys E and F, intense sediment deposition occurred in the centre of the channel (*c.* $460\,m^2$) while no changes occurred in the profile near the right bank. This process may result in lateral sediment fluxes coming from the higher parts of the bar and oriented toward the side pool associated with the bars (see small deltas visible on Figure 1). Obviously, for these water levels, sediments coming from upstream may also be preferentially oriented laterally.

Discussion

Influence of discharge variations on formation of shorter bars

Since they are formed in a straight channel, the alternate bars migrate downstream and grow laterally due to a radial sediment movement caused by convergent and divergent currents influenced by the topography of the bar (Fujita and Muramoto, 1985; Ashmore, 2009) and probably superimposed dunes. In this study, the migration pattern of the bars followed the direction imposed by the banks. This is to some extent comparable to a 'pinball' trajectory (for instance see bar 4 at the downstream end of the channel). The DEMs of Figure 8 show that the bar pattern or configuration within the channel varied cyclically during time. For instance, the morphological configuration of the channel in 2005 is very close to the configuration in 1999.

The initiation of bar 4 always occurs between T5 and T7. This part of the channel is straight and has no significant geometrical discontinuities. DEMs A to C and N in Figure 8 show that the initiation of bar 4 begins where bar 3 divides into two parts. We propose two possible explanations for this division.

First, it can be assumed that the space between these two sections allows the deposition of sediments eroded from the upstream pool (opposite of the upstream part of bar 3). This process is presumed to trigger sediment overloading (initiation of bar 4) which is enhanced by the locally wider cross-section (with larger β, see Figure 5). Results of T7 scour chains confirm this assumption as follows: migration of bar 3 between surveys I (3070 $m^3 s^{-1}$) and M (1500 $m^3 s^{-1}$), erosion between M and N (155 $m^3 s^{-1}$), initiation of bar 4 after N (inversion of the shape of the cross-section).

The second explanation for the formation of bar 4 concerns the variation in discharge which occurred between surveys M and N. As shown by bathymetrical surveys, sediment transport varied strongly according to water stage and location on the bar during the fall in water level (Rodrigues *et al.*, 2012, and cf. Table II). The central part of the downstream avalanche face of bars migrated downstream during low flows as a slightly reworked progradation front. This is explained by the high critical Shields stress of the sediments in the secondary channel. This process reveals the importance of excess bed shear stress in bar sediment reworking and evolution of the bar pattern (Ashmore, 1991). On the margins, intense sediment reworking often occurs at low discharges. This allows the lateral spreading of the bars, probably reinforced by the transverse slope effect and described previously by Ashworth *et al.* (2000, p. 541) and Carling *et al.* (2000) for other fluvial environments. The resulting effect of this process can be seen in the DEM of survey N which shows that the central part of the new bar 4 is quite high topographically in comparison with its margins where two small channels are present. The higher part of the bar will exert a control by deflection and resistance on flow and sediment transport during the next flood (Claude *et al.*, 2012). At this stage, the constriction of flows on the riffles and small channels can allow armouring which will influence sediment transport and bar instability at the beginning of the next flood (Lisle *et al.*, 1991). The constriction of flows during very low flows will locally increase flow velocity in the lateral pools triggering lateral scouring on the margins of the bars. So, the margins and the central part of the bar may not respond similarly to the fall in water level. This could be due to the difference in elevation between the margins and the centre as well as to lateral sedimentary fluxes from the centre to the margins of the bars. The idea here could be expressed as follows: decreasing discharges are associated to an increase of the width-to-depth ratio β, which in theory is favourable for the development of a higher bar mode (Colombini and Tubino, 1991). The simple physics-based predictor of Crosato and Mosselman (2009) roughly associates multiple-bar configurations (i.e. bar modes higher than one) with width-to-depth ratios larger than 50. Ikeda (1984) reports such configurations to occur at width-to-depth ratios higher than 70 to 100. In the secondary channel under consideration here width-to-depth ratios are high between T6 and T7 where the formation of bar 4 always occurs (see Figure 5). In other words, in this straight part of the secondary channel, low discharges trigger bar 4 development (because of high β values and sediment supply coming from bar 3) whereas subsequent floods allow its migration downstream. The process described here could be interpreted as a generation of new alternate migrating bars triggered by discharge variations. Anyhow, following this finding obtained on the Loire, we assume that, under changing boundary conditions, migrating bars could be generated anew in sandy-gravelly river beds, which means that an arbitrary water course with varying discharges may exhibit specific periods in which migrating alternate bars appear.

Tubino (1991) proposes a ratio $\hat{U}$ between the timescale of the basic unsteadyness of flow and the timescale of bar growth (linear growth rate of perturbations). The average number of days for the rising limb of the hydrographs of Figure 3 was taken as representative of the timescale of the basic unsteadyness of flow (here estimated to 120 days). We estimated the timescale for bar growth in two ways. First, we estimated from a comparison between DEMs A and B that a bar needs about 360 days for growing from zero to half its amplitude. This leads to a ratio $\hat{U}=0.33$. Second, we calculated theoretical growth rates by using a linear model developed along the lines of Struiksma *et al.* (1985) and Struiksma and Crosato (1989). In this way we found representative times from tens to hundreds of days, depending on the empirical closure relations for sediment transport rate and direction. Despite this scatter, the calculations confirmed the order of magnitude of the representative time for bar growth derived from the field measurements. The range of values for $\hat{U}$ thus found corresponds to the conditions at which discharge variations and bar growth interact.

Effect of non-uniformities in channel width on alternate bars

Although the role of the bank orientation on bar formation has already been shown by theoretical and experimental investigations, field studies rarely investigate this point (Welford, 1994). The channel studied here exhibited both non-migrating and migrating alternate bars. The non-migrating bars 1 and 2 in the upstream part of the channel are controlled by local non-migrating geometrical forcings: bar 1 by the river curvature upstream of the secondary channel and bar 2 by an asymmetrical narrowing of the channel as well as a lee effect produced by the presence of bar 1. Bar 3 may represent a transitional form as its upstream part is forced by a change in channel direction immediately downstream of the chute, whereas its downstream tail migrates in concord with the migrating bars 4 and 5 that are farther away from local non-migrating geometrical forcings. Its elongation can be seen as non-migrating bar development, whereas its subsequent division into bars 3a and 3b during surveys A, J and M can be seen as a generation of smaller migrating bars. As shown by Figure 8, the migration of bars 4 and 5 concerns displacement of the whole bedform rather than elongation. In the secondary channel investigated, the height of bars did not vary significantly with the width-to-depth ratio as indicated by the bar theory. However, a spreading of some of the bars downstream could be perceived during flood events. Adjustments in bar wavelength can be associated with non-linear effects as the bars grow to finite amplitude (Lewin, 1976; Fujita and Muramoto, 1985; Nelson, 1990).

Both bathymetrical and scour-chain surveys show that the formation of bar 3 occurs immediately downstream of the chute where the channel direction changes. So, the sharp bank-line angles associated with the chutes act as local geometrical forcings. The mechanisms underlying the development of the bar observed in the Loire may be more complex, however, than captured by the equations of the linear model. For instance, flow separation may cause an eddy immediately downstream of the angle, trapping sediments in a way similar to what Bulle (1926) observed in his experiments.

The chute located in the downstream part of the channel also plays a significant role in the migration of bar 4 (see Figure 8), inducing its division into two smaller macroforms. Results provided by scour chains show that the chute is partly responsible for the migration of the bar towards the northwest (NW).

The strong control exerted by the chutes on bar dynamics is reinforced by the presence of consolidated banks which prevent lateral adjustments of the channel. Moreover, remnants of former groynes at the downstream end of the channel are also likely to disturb the migration of the bars near the confluence with the main channel. Here we show that the presence of the chutes can have different consequences for bar development and dynamics. Chutes can trigger bar development (bar 3) or bar division (bar 4).

Dune and bar interactions for unsteady flows

Flow stage constitutes a main control on bar migration celerity (Table II). This complies with the result from linear bar theory that bar celerity increases with increasing intensity of sediment transport and decreasing flow depth. Therefore, bars migrate faster as flow discharge increases. However, the effect of superimposed dunes on the celerity of alternate bars is not trivial, because opposed conclusions may result from simple reasoning that the bar celerity will scale with the ratio of sediment transport rate to flow depth. A higher hydraulic resistance due to superimposed dunes produces larger flow depths, which would imply a lower bar celerity. However, larger flow depths imply also larger sediment transport rates as a result of higher Shields parameter values, which would imply a higher bar celerity. Exercises with the linear model developed along the lines of Struiksma *et al.* (1985) and Struiksma and Crosato (1989) show the theory to predict, as a net result, that bar celerity decreases as the hydraulic resistance increases.

For the channel studied here, the hysteresis effects of dune height yield significant differences in roughness according to the flood stage (cf. Paarlberg *et al.*, 2010). By increasing rapidly their heights and lengths (hence flow resistance) during the rising limb of the flood on all migrating and non-migrating bars, the dunes certainly affect bedload transport rates reaching the bar front (see Figure 12). However, it is difficult to separate the role played by flow variation from the effect of superimposed dune roughness on bar celerity. The correlation between the reduction of bar celerity and the increase of dune amplitude could also be given the alternative interpretation that the two effects are both driven directly by the variation of flow regime, instead of one being the cause of the other.

The transverse slope of the river bed influences the morphological parameters of the dunes during floods on the steepest bars such as bar 3. On this bar dune height evolved with the flow depth (Figure 14, cf. Yalin, 1977; Julien and Klaassen, 1995). This trend has not been observed on the other bars, most likely because their cross-sections were less asymmetrical.

During the falling limb of the hydrograph, dunes adapt their height and length differently according to the bar considered. This can be ascribed to local gravitational effects triggered by the transverse slope of the bar (Fujita and Muramoto, 1985). Moreover, Dietrich and Smith (1984) showed that the transverse slope on a point bar can induce an oblique direction of sediment fluxes which allows a larger quantity of sediments to reach the dunes located downslope.

The average elevation of the bars and the duration of the falling limb may also influence the morphological adaptation of dunes (e.g. bars 3 to 5 and bar 2).

The result of the reworking process is also visible in the internal structure of preserved sediments with decreased set size upward, which can be explained by the adjustment of bedforms to new hydraulic conditions. More specifically, the duration of the fall in water level and the topographical position of bars in the channel may influence the thinning-upward coset of cross-bedding (Jones, 1977) associated with the decrease in dune height in shallower flows (Best *et al.*, 2003). The erosion of dunes at the end of the flood constitutes a new sediment supply directed towards the margins of the bar where a new slipface can be built at an angle of repose associated with large plane cross bedding (Best *et al.*, 2003; Lunt and Bridge, 2004). A similar process has been shown by Rice *et al.* (2009) to cause the initiation of secondary bars on the Fraser River (Canada).

Conclusion

The formation, dynamics and generation of new shorter alternate bars were analysed for various discharge conditions in a secondary channel of the Loire River where both migrating and non-migrating bars were present. The results of this field study were analysed to show to which extent the processes occurring in a full-scale river can be compared to the bar theory.

The first question considered concerns the effect of discharge variations on potential generation of new migrating alternate bars from time to time. During low flows, the increasing width-to-depth ratio (β values higher than 100) and the lateral sediment reworking allow the shifting of the bar regime towards a higher bar mode. Hence, the formation of less elevated new bars is made possible (DEMs A and N, Figure 8). This process, which involves a lateral spreading of the migrating bars influenced by the transverse slope and the deflection exerted by bars already present, seems to be governed by discharge variation but also by the spatial distribution of bars in the secondary channel.

The hypothesis that new small bars can be generated during low flows is supported by the intense reworking of the sandy-gravelly bar sediments during the falling limb of the floods and due to relatively high Shields stress values. The bar smoothing and spreading occurring at low flows was also shown by the stratigraphical architecture of deposits. Once formed, the newly generated bar will grow and migrate downstream.

The second question addressed in this study focuses on the role played by the channel geometry in the formation of alternate bars. The presence of chutes induced by changes in the channel planform could be a cause of bar instability and initiation. The initiation of some of the migrating bars occurs due to a geometrical discontinuity in the channel banks (like non-migrating bars) as shown by Struiksma *et al.* (1985). Such bars may be split into shorter bars after elongation and then migrate downstream (e.g. bar 3 of the present study).

The migration pattern of bars present in the secondary channel is cyclic (DEMs of surveys B and N on Figure 8), and mainly influenced by the orientation of the banks, the width-to-depth ratio and discharge variations.

The third and last question of this study regarded the effect of superimposed dunes on bar migration. The celerity of migrating bars (maximum value recorded was equal to 6.6 m day^{-1}) differed according to location on the bar front and is mainly influenced by the reduction in discharge. In a lesser way, the steepness of dunes and resulting flow resistance (k_{dunes}) may also influence the migration of bars. The evolution of dune height and length during the floods investigated was the same for all the bars during the rising limb of the hydrograph but differed according to the bar considered during the falling limb.

Our study shows that knowledge obtained from laboratory flume experiments and idealized mathematical theories can help in understanding the phenomena that occur in the complex setting of real rivers. Conversely, the analysis of field data reveals the extent to which idealized theories are valid in real rivers, the morphological configurations of real rivers being much more complex than experimental and theoretical conditions. Yet we feel that this is only a first step in understanding the interactions between bars and dunes and the effects of unsteady flows on alternate bars. The present study did not allow a complete testing of the theory. We recommend further research through coupling field surveys, laboratory experiments, numerical modelling and theoretical analysis. Future field research is needed to explain the initiation of smaller migrating bars in straight parts of channels and flow dynamics in the chutes, as we found these to exert a significant control on migrating or non-migrating bar formation. Another research question to be addressed concerns the effects of dunes on bars celerity, considering both flow resistance and sediment supply reaching the bar front). A promising theoretical approach is the combined stability analysis for dunes and bars by Colombini and Stocchino (2011).

Acknowledgements—This work was initiated and partly funded by the Agence de l'Eau Loire-Bretagne (J.-N. Gautier). Data from Voies Navigables de France (E. Guillot), Gip Loire-Estuaire (S. Aumenier, C. Bertier, P. Bona), DREAL Pays de la Loire (N. Ampene) and DREAL Centre (S. Braud) were used. P. Peeters (Hydratech) is acknowledged for the data of flow dynamics modelling. Field investigations were carried out with the help of L. Pacaud, J. Ayrault and Y. Guerez, and grain-size analyses were performed by J.-P. Bakyono and I. Pene (University F. Rabelais, Tours). The contribution of the second author was supported by REFORM 'Restoring Rivers for Effective Catchment Management' (EUs 7th FP Grant Agreement No. 282656).

The authors are grateful to M. De Linares (Artelia) and P. Belleudy (University J. Fourier, Grenoble) for their valuable comments during this work. B. Gandubert (University of Tours) is acknowledged for his help during the analysis of dunes data. This paper is dedicated to the authors' friend J.J. Peters (MariMorph) who sadly passed away in January 2012. The present study is part of the Plan Loire Grandeur Nature masterplan.

References

Allen JRL. 1984. Sedimentatry Structures: Their Character and Physical Basis. Developments in sedimentology. Elsevier: Amsterdam; 1256 pp.

Ashley GM. 1990. Classification of large-scale subaqueous bedforms: a new look at an old problem. *Journal of Sedimentary Petrology* **60**: 160–172.

Ashmore P. 1991. How do gravel-bed rivers braid? *Canadian Journal of Earth Sciences* **28**: 326–341.

Ashmore PE. 2009. Intensity and characteristic length of braided channel patterns. *Canadian Journal of Civil Engineering* **36**: 1656–1666.

Ashworth PJ, Best JL, Roden J, Bristow CS, Klaassen GJ. 2000. Morphological evolution and dynamics of a large, sand braid-bar, Jamuna River, Bangladesh. *Sedimentology* **47**: 533–555.

Babonaux Y. 1970. Le lit de la Loire: étude d'hydrodynamique fluviale. Bibliothèque nationale: Paris; 252 pp.

Bertoldi W, Tubino M. 2007. River bifurcations: experimental observations on equilibrium configurations. *Water Resources Research* **43**: 1–10.

Best JL, Ashworth PJ, Bristow CS, Roden J. 2003. Three-dimensional sedimentary architecture of a large, mid-channel sand braid bar, Jamuna River, Bangladesh. *Journal of Sedimentary Research* **73**: 516–530.

Blondeaux P, Seminara G. 1985. A unified bar-bend theory of river meanders. *Journal of Fluid Mechanics* **157**: 449–470.

Bridge JS. 2003. R*ivers and Floodplains: Forms, Processes, and Sedimentary Record*. Blackwell: Oxford; 491 pp.

Brossé R. 1982. Les processus sédimentaires dans le fleuve Loire. Université d'Angers: Angers; 350 pp.

Bulle H. 1926. Untersuchungen über die Geschiebeableitung bei der Spaltung von Wasserläufen. VDI Verlag: Berlin (in German).

Callander RA. 1969. Instability and river channels. *Journal of Fluid Mechanics* **36**: 465–480.

Carling PA, Gölz E, Orr HG, Radecki-Pawlik A. 2000. The morphodynamics of fluvial sand dunes in the River Rhine, near Mainz, Germany. I. Sedimentology and morphology. *Sedimentology* **47**: 227–252.

Church M, Rice SP. 2009. Form and growth of bars in a wandering gravel-bed river. *Earth Surface Processes and Landforms* **34**: 1422–1432.

Claude N, Rodrigues S, Bustillo V, Bréheret J-G, Macaire J-J, Jugé P. 2012. Estimating bedload transport in a large sand–gravel bed river from direct sampling, dune tracking and empirical formulas. *Geomorphology* **179**: 40–57.

Colombini M, Seminara G, Tubino M. 1987. Finite amplitude alternate bars. *Journal of Fluid Mechanics* **181**: 213–232.

Colombini M, Stocchino A. 2011. A linear analysis of 3D dunes and bars. *RCEM2011, Proceedings, 7th Symposium on River, Coastal and Estuarine Morphodynamics*, Shao X, Wang Z, Wang G (eds), September 6–8, 2011, Tsinghua University, Beijing, China.

Colombini M, Tubino M. 1991. Finite-amplitude free bars. A fully nonlinear spectral solution. In Sand Transport in Rivers, Estuaries and the Sea, Soulsby R, Bettes R (eds). A.A. Balkema: Brookfield. VT; 163–169.

Crosato A, Getaneh AA, Desta FB, Uijttewaal WSJ, Le U. 2010. Long-duration laboratory experiment of slow development of steady alternate bars. In *Proceedings of the International Conference on Fluvial Hydraulics – River Flow 2010*; 1035–1039.

Crosato A, Mosselman E. 2009. Simple physics-based predictor for the number of river bars and the transition between meandering and braiding. *Water Resources Research* **45**: W03424.

Crosato A, Mosselman E, Desta FB, Uijttewaal WSJ. 2011. Experimental and numerical evidence for intrinsic nonmigrating bars in alluvial channels. *Water Resources Research* **47**: W03511. DOI: 10.1029/2010WR009714

De Linares M. 2007. Modélisation numérique bidimensionnelle du transport solide et de la dynamique fluviale: validation sur deux sites en Loire et sur l'Arc. Joseph Fourier: Grenoble; 96 + annexes pp.

De Linares M, Belleudy P. 2007. Critical shear stress of bimodal sediment in sand–gravel rivers. *Journal of Hydraulic Engineering* **133**: 555–559.

Dietrich WE, Smith JD. 1984. Bed load transport in a river meander. *Water Resources Research* **20**: 1355–1380.

Eekhout JPC, Hoitink AJF, Mosselman E. 2013. Field experiment on alternate bar development in a straight sand-bed stream. *Water Resources Research* **49**: 8357–8369. DOI: 10.1002/2013

Flemming BW 1988. Zur Klassifikation subaquatischer, strömungstransversaler Transportkörper. *Bochumer Geologische und Geotechnische Arbeiten* **29**: 44–47.

Folk RL, Ward WC 1957. Brazos river bar: a study of the significance of grain size parameters. *Journal of Sedimentary Petrology* **27**(1): 3–26.

Fujita Y, Muramoto Y. 1985. Experimental study on stream channel processes in alluvial rivers. *Bulletin Disaster Prevention Research Institute, Kyoto University* **32**(1), 288, 49–96.

Fuller IC, Hutchinson E. 2007. Sediment flux in a small gravel-bed stream: response to channel remediation works. *New Zealand Geographer* **63**: 169–180.

Hansen E. 1967. On the Formation of Meanders as a Stability Problem, Progress Report 13, Basic Research. Coastal Engineering. Laboratory, Technical University of Denmark: Lyngby; 9.

Hassan MA. 1990. Scour, fill, and burial depth of coarse material in gravel bed streams. *Earth Surface Processes and Landforms* **15**: 341–356.

Hassan MA, Schick AP, Shaw PA. 1999. The transport of gravel in an ephemeral sandbed river. *Earth Surface Processes and Landforms* **24**: 623–640.

Heritage GL, Milan DJ, Large ARG, Fuller IC. 2009. Influence of survey strategy and interpolation model on DEM quality. *Geomorphology* **112**: 334–344.

Hydra. 2010. Manuel d'analyse – Tome 2: modélisation hydraulique; 50 pp. http://www.hydratec.setec.fr/

Ikeda S. 1984. Prediction of alternate bar wavelength and height. *Journal of Hydraulic Engineering* **110**: 317–386.

Jaeggi MNR. 1984. Formation and effects of alternate bars. *Journal of Hydraulic Engineering* **110**: 142–156.

Jones CM. 1977. Effects of varying discharge regimes on bed-form sedimentary structures in modern rivers. *Geology* **5**: 567–570.

Julien PY, Klaassen GJ. 1995. Sand-dune geometry of large rivers during floods. *Journal of Hydraulic Engineering* **121**: 657–663.

Kleinhans MG, Jagers HRA, Mosselman E, Sloff CJ. 2008. Bifurcation dynamics and avulsion duration in meandering rivers by one-dimensional and three-dimensional models. *Water Resources Research* **44**: 1–31.

Knaapen MAF, Hulscher SJMH, De Vriend HJ, Van Harten A. 2001. Height and wavelength of alternate bars in rivers: modelling vs. laboratory experiments. *Journal of Hydraulic Research* **39**: 147–153.

Lanzoni S. 2000. Experiments on bar formation in a straight flume: 1. Uniform sediment. *Water Resources Research* **36**: 3337–3349.

Lanzoni S, Tubino M. 1999. Grain sorting and bar instability. *Journal of Fluid Mechanics* **393**: 149–174.

Latapie A. 2014. Assessing channel response of a long river influenced by human disturbance, *Catena* **121**: 1–12.

Latapie A, Camenen B, Paquier A, Rodrigues S, Moatar F. 2009. Morphological evolution of the middle Loire River: definition of geomorphic homogeneous river reaches. In River Coastal and Estuarine Morphodynamics, Vionnet CA, Garcia MH, Latrubesse EM, Perillo GME (eds). CRC Press – Taylor & Francis Group: Santa Fé; vol. **1**, 43–49.

Laronne JB, Outhet DN, Carling PA, McCabe TJ. 1994. Scour chain employment in gravel bed rivers. *Catena* **22**: 299–306.

Leclair SF, Bridge JS, Wang XX. 1997. Preservation of cross-strata due to migration of subaqueous dunes over aggrading and non-aggrading beds: comparison of experimental data with theory. *Geoscience Canada* **24**: 55–66.

Lewin J. 1976. Initiation of bed forms and meanders in coarse-grained sediment. *Geological Society of America Bulletin* **87**: 281–285.

Lisle T, Ikeda H, Iseya F. 1991. Formation of stationary alternate bars in a steep channel with mixed size sediment: a flume experiment. *Earth Surface Processes and Landforms* **16**: 463–469.

Lisle T, Iseya F, Ikeda H. 1993. Response of a channel with alternate bars to a decrease in sediment supply of mixed-size bed load: a flume experiment. *Water Resources Research* **29**: 3623–3629.

Lunt IA, Bridge JS. 2004. Evolution and deposits of a gravelly braid bar, Sagavanirktok River, Alaska. *Sedimentology* **51**: 415–432.

Miall AD. 1996. The Geology of Fluvial Deposits: Sedimentary Facies, Basin Analysis, and Petroleum Geology. Springer: Berlin; 582 pp.

Mosselman E, Tubino M, Zolezzi G. 2006. The overdeepening theory in river morphodynamics: two decades of shifting interpretations. In *Proceedings of the International Conference on Fluvial Hydraulics – River Flow 2006*; 1175–1181.

Moore ID, Grayson RB, Ladson AR. 1991. Digital terrain modelling: a review of hydrological, geomorphological, and biological applications. *Hydrological Processes* **5**: 3–30.

Nelson JM. 1990. The initial instability and finite-amplitude stability of alternate bars in straight channels. *Earth-Science Reviews* **29**: 97–115.

Olesen KW. 1984. Alternate bars in and meandering of alluvial rivers. In River Meandering, Elliott CM (ed.). Proceedings of the Conference on Rivers 1983, New Orleans. American Society of Civil Engineers (ASCE): Reston, VA; 873–884.

Paarlberg AJ, Dohmen-Janssen CM, Hulscher SJMH, Termes P, Schielen R. 2010. Modelling the effect of time-dependent river dune evolution on bed roughness and stage. *Earth Surface Processes and Landforms* **35**: 1854–1866.

Parker G, Johanneson H. 1989. Observations on several recent theories of resonance and overdeepening in meandering channels. In River Meandering, Ikeda S, Parker G (eds), AGU, Water Resources Monograph 12. American Geophysical Union (AGU): Washington, DC; 379–415.

Peters JJ. 1971. La dynamique de la sédimentation de la région divagante du bief maritime du fleuve Congo. Rapport Mateba 7. Laboratoire de Recherches Hydrauliques, Ministére des Travaux Publics: Delmas; 1–120.

Peters JJ. 1978. Discharge and sand transport in the braided zone of the Zaire estuary. *Netherlands Journal of Sea Research* **12**: 273–292.

Reesink AJH, Bridge JS. 2007. Influence of superimposed bedforms and flow unsteadiness on formation of cross strata in dunes and unit bars. *Sedimentary Geology* **202**: 281–296.

Reesink AJH, Ashworth PJ, Sambrook-Smith GH, Best JL, Parsons DR, Amsler ML, Hardy RJ, Lane SN, Nicholas AP, Orfeo O, Sandbach SD, Simpson CJ, Szupiany RN. 2014. Scales and causes of heterogeneity in bars in a large multi-channel river: Rio Parana, Argentina. *Sedimentology* **61**: 1055–1085.

Rice SP, Church M, Wooldridge CL, Hickin EJ. 2009. Morphology and evolution of bars in a wandering gravel-bed river; lower Fraser river, British Columbia, Canada. *Sedimentology* **56**: 709–736.

Rodrigues S, Bréhéret JG, Macaire JJ, Greulich S, Villar M. 2007. In-channel woody vegetation controls on sedimentary processes and the sedimentary record within alluvial environments: a modern example of an anabranch of the River Loire (France). *Sedimentology* **54**(1): 223–242.

Rodrigues S, Bréhéret JG, Macaire JJ, Moatar F, Nistoran D, Jugé P. 2006a. Flow and sediment dynamics in the vegetated secondary channels of an anabranching river: the Loire River (France). *Sedimentary Geology* **186**: 89–109.

Rodrigues S, Claude N, Jugé P, Bréhéret JG. 2012. An opportunity to connect the morphodynamics of alternate bars with their sedimentary products. *Earth Surface Processes and Landforms* **37**: 240–248.

Rodrigues S, Gautier JN, Peters JJ. 2006b. Sediment dynamics in anabranches of the Loire river: the study case of Ingrandes (France). In River Flow 2006, Ferreira RML, Alves ECTL, Leal JGAB, Cardoso AH (eds). Taylor & Francis: Lisbon; vol. **2**, 1293–1300.

Schielen RMJ, Doelman A, Swart HE. 1993. On the non-linear dynamics of free bars in straight channel. *Journal of Fluid Mechanics* **252**: 325–356.

Seminara G, Tubino M. 1989. Alternate bars and meandering: free, forced and mixed interactions. In River Meandering, Ikeda S, Parker G (eds). American Geophysical Union (AGU): Washington, DC; 267–320.

Smith ND. 1974. Sedimentology and bar formation in the upper Kicking Horse River, a braided outwash stream. *Journal of Geology* **82**: 205–223.

Struiksma N, Crosato A. 1989. Analysis of a 2-D bed topography model for rivers. In River Meandering, Ikeda S, Parker G (eds), Water Resources Monograph 12. American Geophysical Union (AGU): Washington, DC; 153–180.

Struiksma N, Olesen KW, Flokstra C, de Vriend HJ. 1985. Bed deformation in curved alluvial channels. *Journal of Hydraulic Research* **23**(1): 57–79.

Ten Brinke WBM, Wilbers AWE, Wesseling C. 1999. Dune growth, decay and migration rates during a large-magnitude flood at a sand and mixed sand–gravel bed in the Dutch Rhine River system. In Fluvial Sedimentology VI: International Association of Sedimentologists, Smith ND, Rogers J (eds), Special Publication 28. Blackwell: Oxford; 15–32.

Tubino M. 1991. Growth of alternate bars in unsteady flows. *Water Resources Research* **27**: 37–52.

Tubino M, Repetto R, Zolezzi G. 1999. Free bars in rivers. *Journal of Hydraulic Research* **37**: 759–775.

Tubino M, Seminara G. 1990. Free-forced interactions in developing meanders and suppression of free bars. *Journal of Fluid Mechanics* **214**: 131–159.

Tuijnder AP, Ribberink JS, Hulscher SJMH. 2009. An experimental study into the geometry of supply-limited dunes. *Sedimentology* **56**: 1713–1727.

Van Der Mark CF, Blom A, Hulscher SJMH. 2008. Quantification of variability in bedform geometry. *Journal of Geophysical Research* **113**: F03020.

Van Rijn LC. 1984. Sediment transport, part II: bed forms and alluvial roughness. *Journal of Hydraulic Engineering* **110**: 1733–1754.

Van Rijn LC. 1993. Principles of Sediment Transport in Rivers, Estuaries and Coastal Seas. Aqua Publications: Amsterdam; 700 pp.

Villard P, Church M. 2005. Bar and dune development during a freshet: Fraser River Estuary, British Columbia, Canada. *Sedimentology* **52**: 737–756.

Welford MR. 1994. A field test of Tubino's (1991) model of alternate bar formation. *Earth Surface Processes and Landforms* **19**: 287–297.

Wilbers AWE, Ten Brinke WBM. 2003. The response of subaqueous dunes to floods in sand and gravel bed reaches of the Dutch Rhine. *Sedimentology* **50**: 1013–1034.

Yalin MS. 1977. Mechanics of Sediment Transport. Pergamon Press: Oxford; 290 pp.

Zolezzi G, Bertoldi W, Tubino M. 2006. Morphological analysis and prediction of river bifurcations. In Braided Rivers, Sambrook-Smith GH, Best JL, Bristow CS, Petts GE (eds), Blackwell: Oxford; 233–256.

Zolezzi G, Guala M, Termini D, Seminara G. 2005. Experimental observations of upstream overdeepening. *Journal of Fluid Mechanics* **531**: 191–219.

Zolezzi G, Seminara G. 2001. Downstream and upstream influence in river meandering; Part 1, general theory and application to overdeepening. *Journal of Fluid Mechanics* **438**: 183–211.

